A WIND TUNNEL INVESTIGATION OF THE HYDRODYNAMIC STABILITY OF A MANNED UNDERWATER STATION IN OCEAN CURRENTS.

by

Robert Louis Ditchey

United States
Naval Postgraduate School

THESIS

A WIND TUNNEL INVESTIGATION OF THE HYDRODYNAMIC STABILITY OF A MANNED UNDERWATER STATION IN OCEAN CURRENTS

by

Robert Louis Ditchey

October 1969

A Wind Tunnel Investigation of the Hydrodynamic Stability of a Manned Underwater Station in Ocean Currents

by

Robert Louis Ditchey
Lieutenant, United States Navy
B.S., United States Naval Academy, 1962

Submitted in partial fulfillment of the
requirements for the degree of

MASTER OF SCIENCE IN AERONAUTICAL ENGINEERING

from the

NAVAL POSTGRADUATE SCHOOL
October 1969

ABSTRACT

The hydrodynamic stability of an underwater station was studied using wind tunnel models. Rigid model force and moment coefficients were obtained for various orientations of the station in three dimensions. The unsteady motion of the station in cross currents was investigated with a dynamically similar model. Color 8 mm pictures and amplitude-time traces of the unsteady motion were obtained.

TABLE OF CONTENTS

LIST OF TABLES

LIST OF FIGURES

LIST OF SYMBOLS

A	Projected frontal area (characteristic area)
α	Pitch angle
$\dot{\alpha}$	Pitch angle rate, $\frac{\partial \alpha}{\partial t}$

Force Coefficients:

C_D	Drag coefficient, $\frac{D}{qA}$
C_F	Side force coefficient, $\frac{F}{qA}$
C_L	Lift coefficient, $\frac{L}{qA}$

Moment Coefficients:

C_M	Pitching moment coefficient, $\frac{M}{qAd}$
C_N	Yawing moment coefficient, $\frac{N}{qAd}$

Stability derivatives:

C_{M_α}	$\frac{\partial C_M}{\partial \alpha}$
$C_{M_{\dot{\alpha}}}$	$\frac{\partial C_M}{\partial \left(\frac{\dot{\alpha} d}{2V}\right)}$
C_{N_ψ}	$\frac{\partial C_N}{\partial \psi}$
$C_{N_{\dot{\psi}}}$	$\frac{\partial C_N}{\partial \left(\frac{\dot{\psi} d}{2V}\right)}$
C_{F_ψ}	$\frac{\partial C_F}{\partial \psi}$
$C_{F_{\dot{y}}}$	$\frac{\partial C_F}{\partial \dot{y}}$

D	Drag force
d	Mean diameter (characteristic length)
F	Side force
g	Gravitational constant
I_{zz}	Mass moment of inertia
k	Spring constant
λ	Scale ratio, $\frac{d_{model}}{d_{prototype}}$
L	Lift force
M	Pitching moment
m	Mass
N	Yawing moment
N_{RE}	Reynolds number, $\frac{Vd}{\upsilon}$
υ	Kinematic viscosity
υ^*	Dimensionless kinematic viscosity, $\frac{\upsilon_{salt\ water}}{\upsilon_{air}}$
ζ	Damping ratio, dimensionless
ρ	Density
q	Dynamic pressure, $\frac{1}{2}\rho V^2$
T	Tension of cable
t	Time
τ	Dimensionless time, $t\left(\frac{2V}{d}\right)$
V	Velocity
V^*	Dimensionless velocity, $\frac{V_{model}}{V_{prototype}}$
W	Weight
ω_n	Natural frequency of yaw mode

$\bar{\omega}_n$	Dimensionless frequency of yaw mode $= \frac{d}{2v}\omega_n$
ψ	Yaw angle
$\dot{\psi}$	Yaw angle rate, $\frac{\partial \psi}{\partial t}$
X, Y, Z	Coordinates, displacement
Ω_n	Natural frequency of lateral translational mode
$\bar{\Omega}_n$	Dimensionless frequency of lateral translational mode

Subscript:

m	model
p	prototype

ACKNOWLEDGMENT

The writer wishes to express his sincere appreciation to those persons whose assistance and cooperation contributed greatly to the completion of this study, in particular, to Mr. Gilbert DeVlaminck, who fabricated the MUS models, to Mr. Stan Johnson and Mr. Ted Dunton of the Naval Postgraduate School Department of Aeronautics, and to the technicians of the Department of Aeronautics.

The writer is especially indebted to his thesis advisor, Dr. Louis V. Schmidt, for his guidance in this research effort.

I. INTRODUCTION

The purpose of this study was to investigate the hydrodynamic stability of a manned underwater station when the station is fully submerged and subject to cross currents. The concept of a manned underwater station, or MUS, has been investigated by General Dynamics Corporation, Electric Boat Division, under contract for the U. S. Naval Civil Engineering Laboratory, Port Hueneme, California (Ref. 1). The present study, which is in support of the earlier MUS work, was sponsored by NCEL under work order WR-8-0128 and was monitored by Dr. Cheng Lung Liu of NCEL Ocean Engineering Department.

The object of the MUS project as stated in Ref. 1 is to develop a deep ocean submergence habitat which will accommodate a five man crew for an operational period of thirty days. The station is to be capable of submergence to depths of 6,000 feet.

As envisioned by General Dynamics, the station would consist of two circular cylinders of unequal diameters and heights. The smaller diameter cylinder is capped with hemispherical ends and will contain a nuclear reactor. The larger diameter cylinder is capped with spherical ends which are fitted to the cylinder by conical, tangential shells. (Fig. 1) The habitat cylinder will have five decks and is the working space for the crew.

Since these cylinders are designed only for a vertical orientation, a large ballast tank completely encircles both cylinders. The design of this tank is based in part on weight and balance considerations.

The station is not equipped with a propulsion device although it does have ballast and buoyancy control equipment. The concept of the station is somewhat unique and the MUS may best be described as an elevator. In concept, the station is to be towed on the surface to a pre-selected site by a support vessel. When the operations site is reached, the station will be manned and an emplacement procedure will commence. The MUS will utilize an anchor and cable arrangement to pull itself to the bottom in bootstrap fashion. It is equipped with a winch (located on the main ballast tank) and attendant systems for control.

When submerged, the MUS will maintain a slight positive buoyancy at all times. The anchor will first be lowered to the ocean bottom while the MUS holds on the surface. Once the anchor is in place, the buoyancy of the MUS is reduced and winchdown begins. As the winch retrieves the cable, the MUS will haul itself to the bottom. The recovery cycle, i.e., the ascent to the surface, is just the reverse of this procedure.

It is primarily with the emplacement and recovery operations that this study is concerned. When the MUS is in the mid-water column, it may well be subjected to a cross flow caused by deep ocean currents. Evidence exists to expect such currents throughout the water column, having a magnitude of 0.1 to 0.5 knots.

If such currents were to exist, it would be reasonable to expect the MUS to be forced into motion until equilibrium is attained. Such motion could be translational or rotational and perhaps oscillatory in nature. Since the MUS is restrained only by a single cable (to the anchor), the only other stabilizing elements are:

1. The buoyancy couple caused by the displacement of the meta center relative to the center of gravity.
2. Hydrodynamic stabilization, i.e., the geometry of the station, including such extremities as the legs and pads.
3. The inertial resistance to motion (moment of inertia)

Another aspect of the MUS recovery cycle which necessitated a stability investigation was that of emergency ascent. It was proposed that, in the event of an emergency such as cable jamming or bottom entrapment of the support pads, a free ascent could be accomplished by cutting the cable (with explosive cutters) and/or jettisoning the support pads and legs. Since these are in fact stabilizing devices, such an ascent could only be feasible if the resulting configuration of the MUS provided sufficient stabilization.

The objectives of the experiments reported herein were twofold, namely:

a. To establish by means of rigid model wind-tunnel tests the pertinent dimensionless force and moment coefficients for the MUS at various orientations, and
b. To determine the dynamic behavior using a "partial mode" dynamic model, and in particular to note the existence of any self-induced and/or vortex-induced oscillations.

In this investigation, the MUS was represented by an 0.0209 scale model. Reynolds numbers were matched between model and prototype so that aerodynamic measurements on the scale model were applicable to the hydrodynamic traits of the prototype.

One should note that the MUS configuration is still in the early design stages, hence the results obtained in this study should have as a goal the possible application to other configurations. However,

accurate forecasting tends to be uncertain because the bluff-body features of these configurations do not interact in a linear manner. The testing accomplished in this study was relatively easy, and other configurations could be studied using a similar approach.

II DISCUSSION

A. DESCRIPTION OF MODELS AND EXPERIMENTAL PROCEDURE

The investigations described herein upon the 0.0209 scale MUS models were performed at the Naval Postgraduate School (NPS) low-speed wind tunnel facilities. The force and moment measurements were conducted on the "rigid" model in the Aerolab 32 in. x 45 in. wind tunnel while the scaled dynamic model was tested in the West Coast Research 48 in. x 60 in. wind tunnel.

The "rigid" model was linearly scaled and was fabricated from an overlay of Honduras mahogany upon an aluminum spar or reinforcing plate (Fig. 6). The purpose of the spar plate was to make possible the attachment of the support arms and tail sting at prelocated or orientations of the model. It was possible to position the model in a multitude of ways upon the conventional three strut support system so that representative yaw and pitch attitudes could be obtained for an angle range of $\pm 180^{\circ}$ and $\pm 90^{\circ}$ respectively. Figure 5 presents a sketch of the model including pertinent dimensional data relative to the force model, while Figures 11 to 44 show the model installed in the wind tunnel at various orientations. The model was tested at dynamic pressures from 3.85 to 57.8 psf (in air) which correspond to prototype velocities in sea water from 0.08 to 0.30 knots (refer to Figure 52 for conversion from model to prototype operating conditions).

The forces and moments were measured upon an Aerolab three-component beam balance (Fig. 10) which had the capability of measuring lift, drag, and pitching moment relative to the wind axes.

The balance limits were:

Component	Limits	Sensitivity
Lift force	± 150 lbs	± 0.010 lbs
Drag force	± 50 lbs	± 0.005 lbs
Pitch moment	± 1000 in-lbs	± 0.050 in-lbs

Care should be exercised in interpreting the meaning of lift and drag forces and pitching moments at some of the extreme model positions, such as when the model has been rolled 90 degrees on the balance, since in this attitude pitch angle changes actually corresponded to model yaw angle changes (Figs. 43 and 44). In this extreme case, lift force and pitching moment correspond to side force and yawing moment respectively. It is unfortunate that the balance system was not readily usable as a six-component type since then it would have been possible to convert the wind axes results to stability or body axes as is frequently done in aircraft analysis.

Data corrections were made for weight tares, while aerodynamic tares to account for the influence of the support system were approximately estimated by measuring the balance force and moments without a model present. Since the model was a relatively bluff body, as compared to a streamlined aircraft configuration, these approximations were considered as being reasonable.

The dynamic model tests may be described as "partial mode" tests since only selected degrees of freedom were investigated. The modes investigated included lateral and axial translation and yaw rotation. The tests were performed upon two 0.0209 scale models, one made from balsa and the other from sugar pine (Figs. 7, 8, and 9).

The balsa model had as its purpose an initial observation of the model's dynamic behavior and an experimental confirmation of the yawing moment static trim points. The full scale weight and weight distribution table for the MUS from Ref. 1 was used as a basis for design of the pine model. By using a component approach, the full scale weights and weight distribution were scaled to obtain the desired mass moment of inertia for the pine model. Removable lead inserts were utilized to allow a variation of mass and mass moment of inertia. The balance of the model about the desired center of gravity location was checked experimentally, while the mass moment of inertia was determined by utilizing the principle of the torsional pendulum. An object having a known moment of inertia, namely a solid steel cylinder of given weight and geometry, was suspended on an 0.037 inch diameter steel piano wire of known length. The oscillation frequency was then measured which in turn allowed the determination of the wire's shear modulus of rigidity. From the physical properties of the wire (diameter, length, and shear modulus), and the measured free vibration oscillation frequencies, it was possible to determine the mass moment of inertia of the model. Table II lists the physical properties of the dynamic models tested.

A narrow diameter tube was inserted along the vertical axis (through the assumed prototype center of gravity) in order to shield the dynamic model from the support wire. The model was suspended on an 0.037 inch diameter steel piano wire which was fixed to supports external to the tunnel. (Figs. 56 through 59) The wire was preloaded to 50 lbs. tension by means of turnbuckles, and the tension was frequently checked by using a standard rigging tensiometer. Initially, only the taut wire support was used, but later tests were conducted

with the translational degrees of freedom removed by means of local tie-down constraints. In addition, the last sequence of dynamic model tests were provided with an electrical angle sensing potentiometer in order to allow time-history traces to be made of the angular motion. (Figs. 60 and 61)

Motion picture photography of the dynamic model tests was accomplished by using a mirror arrangement. An adjustable mirror was mounted to the tunnel wall above the model so that overhead photography was possible. The later tests involved simultaneous photography and electrical data collecting. (Table VI)

B. SCALING CONSIDERATIONS

The scale of the models (0.0209) was established on the basis of the largest model compatible with the wind tunnel test section size and velocity range in combination with a Reynolds number match between model and prototype.

For the prototype design with an ocean current of 0.3 knots in salt water, an estimate of full scale Reynolds number would be

$$N_{RE} = \frac{V_p d_p}{\upsilon_p} = \frac{(0.3 \text{ KTS} \times 1.69 \frac{\text{fps}}{\text{KT}})(14.93 \text{ ft})}{(0.17 \times 10^{-4} \text{ ft}^2/\text{sec})}$$

$$N_{RE} = 4.45 \times 10^5 \qquad \text{(prototype in salt water)}$$

The above Reynolds number is based upon a mean diameter of 14.93 feet. An 0.0209 scale model (λ = 0.0209 = scale ratio) would satisfy the prototype Reynolds number condition above at a tunnel velocity of

$$V_m = \frac{\upsilon_m}{d_m} N_{RE} = \frac{(1.58 \times 10^{-4} \frac{\text{ft}^2}{\text{sec}})(4.45 \times 10^5)}{(0.313 \text{ ft})} = 225.4 \text{ fps}$$

which corresponds to a tunnel dynamic pressure of 60.3 psf. The ratio of model to prototype velocities is 443 under the assumption of equivalent Reynolds numbers.

The mass moment of inertia scaling of the dynamic model was established by the free vibration equation in the yaw mode. As an approximation, one may consider the slope of the C_N vs ψ curve to be linear in the immediate neighborhood of a zero moment static trim position.

The total yawing moment may be approximated by the sum of the linearized static term and a term due to the dimensionless angle rate $\left(\frac{\dot{\psi} d}{2V}\right)$.

$$C_N = \left[C_{N_\psi}\right]\psi + \frac{d}{2V}\left[C_{N_{\dot{\psi}}}\right]\dot{\psi} \qquad \ldots\ldots(1)$$

Multiplying C_N by (qAd) to obtain physical units, then the free vibration equation in yaw is:

$$I_{zz}\frac{d^2\psi}{dt^2} - (qAd)\left(\frac{d}{2V}\right)C_{N_{\dot{\psi}}}\frac{d\psi}{dt} - (qAd)C_{N_\psi}\psi = 0 \qquad \ldots\ldots(2)$$

where: I_{zz} = Mass moment of inertia, taken about the z axis.

Dividing through by I_{zz} and introducing the dimensionless time, τ where: $\tau = \frac{t}{\left(\frac{d}{2V}\right)}$

then

$$\left(\frac{2V}{d}\right)^2\frac{d^2\psi}{d\tau^2} - \frac{qAd}{I_{zz}}C_{N_{\dot{\psi}}}\frac{d\psi}{d\tau} - C_{N_\psi}\frac{qAd}{I_{zz}}\psi = 0 \qquad \ldots\ldots(3a)$$

The enforcement of Reynolds number equivalence insures that the dimensionless yawing moment coefficient C_{N_ψ} is identical for both model and prototype. In order to achieve full dynamic similarity,

the nondimensional, natural frequency of the model must be identical with that of the prototype. This argument then defines the scaling law for the mass moment of inertia as shown below.

$$\frac{d^2\psi}{d\tau^2} - \left[\frac{1}{8}\frac{\rho A d^3}{I_{zz}}\left(C_{N_{\dot\psi}}\right)\right]\frac{d\psi}{d\tau} - \left[\frac{1}{8}\frac{\rho A d^3}{I_{zz}}\left(C_{N_{\psi}}\right)\right]\psi = 0 \qquad \text{.....(3b)}$$

This may be compared to the familiar vibration equation

$$\frac{d^2\psi}{d\tau^2} + 2\xi\bar{\omega}_n\frac{d\psi}{d\tau} + \bar{\omega}_n^2\psi = 0 \qquad \text{.....(4)}$$

In order for the equation of motion to describe concurrently the behavior of both model and prototype, each term must equate in model to prototype conversion, therefore

$$\left[\bar{\omega}_n^2\psi\right]_{model} = \left[\bar{\omega}_n^2\psi\right]_{Prototype}$$

or

$$\frac{\rho_m A_m d_m^3 \left(C_{N_\psi}\right)_m \psi_m}{I_{zz_m}} = \frac{\rho_p A_p d_p^3 \left(C_{N_\psi}\right)_p \psi_p}{I_{zz_p}}$$

since $\left(C_{N_\psi}\right)_m = \left(C_{N_\psi}\right)_p$

$\psi_m = \psi_p$

$\frac{A_m}{A_p} = \lambda^2$ $\qquad$ $\frac{d_m^3}{d_p^3} = \lambda^3$

then

$$\frac{\rho_m \lambda^5}{I_{zz_m}} = \frac{\rho_p}{I_{zz_p}}$$

or

$$\frac{I_{zz_m}}{I_{zz_p}} = \left(\frac{\rho_m}{\rho_p}\right)\lambda^5 \qquad \text{.....(5)}$$

if the inertial scaling of above were used, then the non-dimensional frequency would be alike between model and prototype, i.e.,

$$(\bar{\omega}_n)_m = (\bar{\omega}_n)_p$$

Similarly, a check of the damping terms:

$$\left[\frac{\rho A d^3}{I_{zz}} C_N \dot{\psi}\right]_m = \left[\frac{\rho A d^3}{I_{zz}} C_N \dot{\psi}\right]_p$$

will yield the same result by the same argument.

Unfortunately, such scaling was not physically realizable as it would demand a prohibitively light construction of the model.

Returning to the non-dimensional natural frequency, which may be identified in eqn. (3b);

$$\bar{\omega}_n^2 = -\frac{1}{8} \frac{\rho A d^3}{I_{zz}} C_{N_\psi} \qquad \text{.....(4a)}$$

$$\frac{(\bar{\omega}_n^2)_m}{(\bar{\omega}_n^2)_p} = \left(\frac{\rho_m}{\rho_p}\right) \lambda^5 \left(\frac{I_p}{I_m}\right)$$

if the mass moments of inertia were set as:

$$\frac{I_m}{I_p} = \lambda^5$$

then the dimensionless frequencies won't correspond, but will scale as:

$$\frac{(\bar{\omega}_n^2)_m}{(\bar{\omega}_n^2)_p} = \frac{\rho_m}{\rho_p} = 1.23 \times 10^{-3}$$

Considering that dimensionless frequency is by definition:

$$\bar{\omega}_n = \frac{d}{2V} \omega_n$$

one readily obtains that:

$$(\omega_n)_p = \left(\frac{d_m}{d_p}\right)\left(\frac{V_p}{V_m}\right)\left(\frac{\rho_p}{\rho_m}\right)^{\frac{1}{2}} (\omega_n)_m \qquad \text{.....(6)}$$

After substitution of the scaling parameters (cf. Table I), the true frequency scaling becomes:

$$(\omega_n)_p = 0.00134\,(\omega_n)_m$$

For example, if $(\omega_n)_m = 0.70$ cps , then

$$(\omega_n)_p = 0.00134\,(0.70\ \text{cps})\left(60\ \tfrac{\text{sec}}{\text{min}}\right) = 0.0562\ \tfrac{\text{cycles}}{\text{min}}$$

and the prototype period would be 18.1 min/cycle.

Using a quasi-steady argument, enforced by the case where the damping ratio ξ is zero, one may use the above scaling law to convert model frequencies to prototype frequencies for the yaw mode.

In a similar fashion to the above analysis concerning the yaw mode, one may consider the translational mode free vibration equation. In the lateral translational mode, a similar analysis to the yaw mode scaling may be made starting from the free vibration equation,

$$m\ddot{y} - C_{F_{\dot{y}}}(\rho A)\dot{y} + k y = 0 \qquad \text{.....(7)}$$

The damping derivative, $C_{F_{\dot{y}}}$, may be approximated by the quasi-steady assumption in a manner similar to that used by Parkinson, (Ref. 2) when he considered the limit-cycle solution for the galloping transmission line problem. Using the sign convention of Figure 2, one obtains that:

$$C_{F_{\dot{y}}} = + \frac{1}{V} C_{F_\psi}$$

since $\psi \cong + \dot{y}/V$

Substitution of this approximation into equation (7) yields that:

$$\ddot{y} - \frac{\rho A}{mV} C_{F_\psi}\dot{y} + \frac{k}{m} y = 0 \qquad \text{.....(8)}$$

It is convenient to convert equation (8) to dimensionless time, $\tilde{t}$, and dimensionless lateral translation, $\tilde{y}$, where $\tilde{y} = y/d$. Direct substitution plus a slight amount of algebraic simplification yields:

$$\frac{d^2\tilde{y}}{d\tilde{t}^2} - \frac{\rho A d}{4m} C_{F_y} \frac{d\tilde{y}}{d\tilde{t}} + \frac{k}{m}\frac{d^2}{4V^2}\tilde{y} = 0 \qquad \text{.....(9)}$$

Equation (9) may be compared with the second order differential equation; equation (4), in order to identify that in the lateral translational mode, the non-dimensional frequency is:

$$\bar{\Omega}_n = \Omega_n \left(\frac{d}{2V}\right)$$

where $\Omega_n = \sqrt{k/m}$

For the model installation, the spring constant, k, is proportional to the tension T in taut wire support as may be seen in the rear view sketch below:

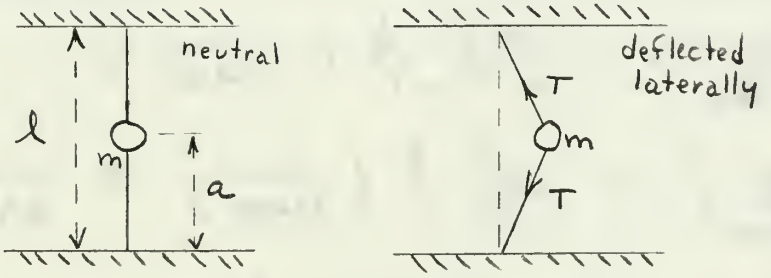

If

$$a = \frac{l}{2} \qquad \frac{y}{a} << 1$$

then

$$k_m = T\left[\frac{1}{a} + \frac{1}{l-a}\right] \cong 4\frac{T_m}{l_m}$$

An approximation for the tethered prototype vehicle may be made on the assumption that the cable tension is equivalent to the buoyancy force. For this case, one would obtain

$$k_p \cong 2\frac{T_p}{l_p}$$

where the tether cable length, ℓ_p , is an equivalent value which may be estimated.

The initial consideration will be to find the true frequency value of the prototype on the assumption of equivalent non-dimensional frequencies, followed by a correction for differences in cable tension. For the case of

$$(\bar{\Omega}_n)_p = (\bar{\Omega}_n)_m$$

it follows that:

$$(\Omega_n)_p = \left(\frac{d_m}{d_p}\right)\left(\frac{V_p}{V_m}\right)(\Omega_n)_m$$

$$(\Omega_n)_p = \frac{1}{21450}(\Omega_n)_m$$

Next, we shall investigate the implications of cable tension. Since $\Omega_n^2 = \frac{k}{m}$, it follows that:

$$\left(\frac{k_p}{k_m}\right)^{\frac{1}{2}} = \left(\frac{m_p}{m_m}\right)^{\frac{1}{2}}\left(\frac{1}{21450}\right)$$

$$\left(\frac{k_p}{k_m}\right)^{\frac{1}{2}} \cong \left(\frac{10^6}{10}\right)^{\frac{1}{2}}\left(\frac{1}{21450}\right) \cong \frac{1}{67.8}$$

or

$$k_p \cong \frac{1}{4600} k_m$$

If cable lengths are approximately given by $\ell_p \cong 600$ ft., $\ell_m \cong 6$ ft, and model cable tension is 50 lbs., then

$$\frac{T_p}{\ell_p} \cong \frac{1}{2300}\frac{T_m}{\ell_m}$$

or

$$T_p \cong 2.18 \text{ lb}$$

Actually it is envisioned that the prototype buoyancy force will be on the order of 100 lbs., hence the corrected frequency would be

$$(\Omega_n)_{p_{corr}} \cong \left(\frac{100}{2.18}\right)^{\frac{1}{2}} (\Omega_n)_p$$

$$(\Omega_n)_p \cong \frac{1}{3170} (\Omega_n)_m$$

Therefore if the lateral translational frequency of the model were about 1 cps, then the representative prototype period would be about 53 minutes per cycle.

In retrospect, the dynamic scaling problem would require simultaneous scaling of mass, mass moment of inertia about the yaw axis, and cable tension. Since this procedure was not initially followed, estimates were made to account for the relative effects of the mismatches.

III. RESULTS

A. RIGID MODEL DATA

Various rigid model plots are included (Figs. 45 through 55). Test runs 1 through 37 indicated that the hydrodynamic coefficients are essentially constant throughout the Reynolds number range under consideration. A large number of Coefficient-Reynolds number plots were obtained (see run schedule, Table VI), and representative plots are shown in Figures 46 through 48 inclusive. The largest values of the hydrodynamic coefficients that were measured, with the corresponding full scale forces and moments, are plotted for comparative purposes in Figure 52. These forces, as compared to the buoyancy force of 100 lbs., are considered to be significant.

A drag coefficient contour plot is included in Figure 45. The drag coefficient values along the ordinate and absisca of this plot were measured in five-degree increments (See also Figs. 49 and 54), while other values were measured in combinations of thirty-degree increments.

The plot of yawing moment coefficient versus yaw angle (Fig. 53) shows that the MUS has two stable trim points in yaw, at zero degrees and 180 degrees, while two unstable trim points exist at 90 and 270 degrees of yaw. It should be emphasized that these are zero yawing moment positions, while the slope indicates the degree of stability. Also note that stable trim did not occur at the orientation for minimum drag.

Direct measurement of the yawing moment vs yaw angle has application to defining the aerodynamic restoring moment term in the

yaw-degree-of-freedom dynamic equation. However, means do not exist for direct measurement of the damping term due to yaw rate. The damping term must be deduced indirectly by observing the time history of decaying yaw oscillation.

The plot of side force versus yaw angle at zero pitch angle is shown on Figure 55. An approximate analytic expression for the variation of side force coefficient is:

$$C_F \cong 0.38 \sin \psi$$

However, the actual plot shows many irregularities in the curve which may be related to the complex flow interactions between the various bluff-body components that comprise the MUS. Especially noteworthy is the rapid unstable trim points, $\psi = \pm 90^\circ$.

It should also be noted that the above expression for side force coefficient will result in the damping term of the lateral translational degree of freedom having a negative value. The consequence of this feature was noted in the dynamic model as a limit cycle type of motion.

B. DYNAMIC MODEL RESULTS

A color 8 mm motion picture film was prepared as a supplement to this report. Part one of the film shows the experiments with the single wire arrangement, and careful observation will show the lateral motion beating phenomenon. In this configuration the model had degrees of freedom both in yaw and lateral translation. The combination of an apparently lightly damped yaw mode plus a negatively damped lateral translation mode produced a complex response with an apparent indication of beating due to the closeness

of the two frequencies. The lateral excitation caused the self-induced nature of the oscillation in yaw, but this did not appear when the lateral constraint was imposed.

Part two of the film shows the instrumented and constrained model experiments. No lateral motion occurred and the damping ratio was small but finite until a dynamic pressure of five or six psf was reached. Strip recorder charts are included. (Fig. 67) Dynamic model data are summarized below in Figs. 62 through 66. The predicted frequencies for the model, shown as estimates on Figs. 62 to 64, are based upon the recognition of frequency from equations (2) and (4a) as:

$$\omega_n = \frac{2V}{d}\bar{\omega}_n = \left[\left(\frac{\rho A d}{I_{zz}}\right)(-C_{N_\psi})\right]^{\frac{1}{2}}$$

Although the predicted frequencies are about 10 to 15 percent higher than measured values, the trends with dynamic pressure are proper and add confirmation to the concept of an equivalent hydrodynamic torsional spring term. It is quite possible that the actual observed frequencies reflect rate dependence of the hydrodynamic torsional spring term on the bluff body.

IV. ANALYSIS

A. STATIC STABILITY

The MUS stability in the pitch mode may be interpreted from Figure 50; i.e., the pitching moment coefficient versus pitch angle plot. This plot was obtained only for zero degrees of yaw. At minus ninety degrees pitch angle, i.e., the ascending mode, the MUS will trim but be statically unstable. While the pitching moment itself is zero at $\alpha = -90^{\circ}$, any increase in pitch angle results in a positive pitching moment which tends to increase the pitch angle further. Similarly, a decrease in pitch angle results in a negative pitching moment. At plus ninety degrees pitch angle i.e. the descending mode, the MUS is again statically unstable. In the neighborhood of zero degrees pitch angle, the MUS has a positive pitching moment coefficient and hence is not trimmed. Therfore, in the absence of the cable constraint, the MUS is statically unstable in the pitch mode. The balsa wood dynamic model was suspended in a manner so as to allow a pitch degree of freedom for one set of exploratory investigations. Its dynamic behavior tended to confirm the preceding conjectures since the stable trim points appeared to be weak and the model was quite prone to rotate in pitch.

In the vertical translation mode the MUS is statically unstable. Referring to Figure 51$\left(\alpha = 0, \quad \psi = 0, C_L \text{ vs } \alpha\right)$, in a direct cross current, the MUS has a negative lift, which will tend to cause the MUS to descend. This in turn would increase the effective pitch angle, and result in a more negative lift.

Figure 53 shows that the station is statically stable in the yaw mode (at zero pitch) at yaw angles of zero and 180 degrees and statically unstable in yaw at 90 and 270 degrees of yaw.

Figure 55 shows that the station is statically unstable in lateral translation at yaw angles of zero and 180 degrees. If a lateral translational velocity occurs, an effective yaw angle is introduced in the nature of sideslip. When this occurs, the side force is such that the lateral translation tends to be further increased (forced).

B. DYNAMIC STABILITY

In the absence of constraints, the experiments indicated that the MUS would be dynamically unstable in all translation modes and in the pitch mode.

The yaw mode appeared to be dynamically stable, as the oscillation amplitude either decreased in time or remained constant. Negative damping ratios were not observed for the range of tunnel speeds used, but it is possible that higher dynamic pressures could have induced negative damping.

The scaling relations for the yaw mode and the lateral translation mode indicate that the natural frequencies of these modes are very widely separated at full scale. This would indicate that the coupling tendency observed in the model experiments would not occur for the full scale MUS. The most important conclusion from scaling considerations is that an oscillation on the model in a wind tunnel on the order of a second per cycle period would scale to the prototype vehicle in water with a period on the order of 20 to 50 minutes per

cycle. Therefore it is quite possible that unusual oscillational behaviors in the tunnel would not be perceptible to the crew enclosed in the MUS because of the low velocities involved.

C. COMMENTS ON MUS CONSTRAINTS

The experimental results indicated that the proposed free ascent mode would be practicable. Considering an assumed stabilized condition where the MUS would be floating freely in any existing current, with cable and pads jettisoned, and in the absence of an unequilibrated buoyancy force, no hydrodynamic force would be generated. If the positive buoyancy force of approximately 100 lbs. were considered, the MUS would be forced into vertical translation and hydrodynamic forces would be generated. In this orientation, the wind tunnel axis position of minus ninety degrees of pitch angle would be applicable (Fig. 2). Assuming that a constant side current existed throughout the water column, the MUS would begin to rise, sensing only the hydrodynamic forces corresponding with $\alpha = -90^{\circ}$. However, in this orientation, both a drag force and a lift force could be generated. If one assumes that the MUS could achieve a vertical velocity of 0.2 knots, from the wind tunnel results, the resulting drag force would be 100 lbs., and the lift force would be zero (Figs. 49, 51, 52). Actually, the resulting drag forces would limit vertical ascent speed to 0.2 knots, if the 100 lb. buoyancy force were maintained. This speed limitation may be verified by cross referencing Figs. 49 and 52. The drag coefficient of 0.7 will result in a drag force of 100 lbs. at 0.2 knots, therefore the drag force will equilibrate the net buoyancy force at 0.2 knots. A check of the pitching moment vs. pitch angle plot (Fig. 50) for this orientation

shows that the MUS would be at an unstable trim point, that is the pitching moment would be zero but the variation of moment with flow angle would not produce a restoring moment. As long as the flow vector remains constant at $\alpha = -90^{\circ}$, the MUS will remain upright. If the flow vector is disturbed from $\alpha = -90^{\circ}$ or more likely, if the MUS begins ascending from an off-vertical orientation, the resulting pitching moment will be in a direction tending to overturn the MUS. This pitching moment would be on the order of 300 ft-lbs. maximum (for a 0.2 knot vertical speed and a 20° off-vertical orientation). Considering the design (buoyancy couple) stability, this slight pitching moment should present no difficulties (ref. 1). That is, the location of the center of buoyancy above the center of gravity results in a stabilizing moment.

Considering the case where the MUS is tethered by the cable in the mid-water column, if side currents exist with a speed of 0.3 knots, a pitching moment would be generated on the order of 1300 ft-lbs. maximum. This would place a side load on the cable attachment point, as the cable would equilibrate the pitching moment. In addition, a yawing moment would exist, having the same order of magnitude. The yawing moment would apply a torsional load to the cable or to the cable attachment point, depending on the actual design, however, the vehicle would tend to align itself to the stable trim point corresponding to $\gamma = 0^{\circ}$ or 180°.

The oscillatory behavior of the model appears to be of no practical consequence to the full scale MUS and probably would not be noticable by the crew. Considering the proposed emplacement procedure, since the principal static equilibrating force that exists to counteract

drag forces (in side currents) is the 100 lbs. buoyancy force, the wind tunnel measurements indicate that a forced descent would result with current speeds as small as 0.2 knots. At this speed, the resulting drag force would be equal to the buoyancy force, and therefore, static equilibration would not be possible.

The restoring force F_x is equal to:

$$F_x = T \sin \gamma$$

Where T = buoyancy force = cable tension

and γ = deflection angle of the cable from the vertical

if $T = 100$ lbs.

for a current speed of 0.15 knots and $C_D = 0.7$

$$D = 60 \text{ lbs. (Fig. 52)}$$

$$\sin \gamma = 0.6$$

$$\gamma = 37^\circ$$

or in other terms, a horizontal translation of 3,600 ft. and a 1,200 ft. descent would occur before static equilibration if 6,000 ft. of cable separated the MUS and its anchor. For this reason, it is recommended that a higher buoyancy force be considered.

The foregoing discussion on forced descent is admittedly overly simplified and does not take into consideration the special effect of catenary behavior of the cable itself. This topic would merit individual study and analysis before a complete discussion of forced descent could be made. It is also recognized that increasing the buoyancy force will create a serious problem involving free ascent terminal velocity. In this respect, a compromise would be involved between stability considerations and ascent problems.

TABLE I

VALUES OF SOME PHYSICAL CONSTANTS

Characteristic area (model)	0.546 ft^2
Characteristic area (prototype)	1248 ft^2
Height of model	1.0 ft
Height of prototype	47.8 ft
Characteristic length (model)	3.75 in
Characteristic length* (prototype)	14.93 ft
Scale ratio, λ	0.0209
λ^2	4.37×10^{-4}
λ^3	9.0×10^{-6}
λ^5	4.0×10^{-9}
ν, salt water	0.17×10^{-4} ft^2/sec
ν, air	1.58×10^{-4} ft^2/sec
ρ_m/ρ_p	1.23×10^{-3}
Dimensionless velocity, V^*	443

*Note: The characteristic length was arbitrarily chosen to be the average or mean of the diameters of the five principal components which comprise the MUS.

TABLE II

Model	Type Construction	Mass (Slugs)	Mass moment of inertia (slugs-ft^2)	Remarks
A	Honduras	Not determined	Not determined	Rigid, force model
B	Balsa	Not determined	0.00080	First dynamic model
C	Pine	0.302	0.01935	Full dynamic model
D	Pine	0.259	0.01706	Two lead inserts removed from C model
E	Pine	0.215	0.01089	Four lead inserts removed from C model

TABLE III: DRAG COEFFICIENT SUMMARY

Yaw Angle	0	30	60	90	120	150	180	210	240	270	300	330
Pitch Angle												
+90	0.87	0.87	0.87	0.88	0.87	0.87	0.87	0.87	0.87	0.87	0.87	0.87
+60	0.67	0.65	0.66	0.66	0.64	0.65	0.70	0.67	0.68	0.69	0.67	0.68
+30	0.70	0.65	0.50	0.43	0.51	0.67	0.73	0.67	0.55	0.46	0.55	0.65
0	0.73	0.63	0.39	0.28	0.38	0.63	0.70	0.60	0.44	0.30	0.45	0.64
-30	0.68	0.62	0.50	0.44	0.47	0.58	0.66	0.60	0.52	0.42	0.51	0.61
-60	0.72						0.70	0.69				
-90	0.70	0.70	0.70	0.70	0.70	0.70	0.70	0.70	0.70	0.70	0.70	0.70

TABLE IV: LIFT COEFFICIENT SUMMARY

Yaw Angle / Pitch Angle	0	30	60	90	120	150	180	210	240	270	300	330
+90	+0.13	+0.02	+0.03	-0.04								
+60	+0.25	+0.28	+0.32	+0.32	+0.25	+0.19	+0.15	+0.16	+0.20	+0.30	+0.28	+0.24
+30	-0.13	-0.07	0.00	+0.02	-0.04	-0.10	-0.14	-0.05	0.00			
0	-0.12	-0.14	-0.02	-0.03	-0.04	-0.07	-0.05	-0.05	-0.04			
-30	+0.18	+0.14	+0.05	0.00	+0.02	+0.17	+0.23	+0.12	+0.08			
-60	+0.01						-0.03	-0.07				
-90	0.00											

TABLE V: PITCHING MOMENT COEFFICIENT SUMMARY

Yaw Angle	0	30	60	90	120	150	180	210	240	270	300	330
Pitch Angle												
+90	+0.01			0.00								
+60	-0.03	-0.01	0.00	+0.01	-0.02	-0.03	-0.04	-0.02	0.00	+0.03	+0.03	0.00
+30	+0.09	+0.12	+0.06	+0.06	+0.18	+0.15	+0.13	+0.13	+0.08			
0	+0.20	+0.09	+0.05	+0.00	+0.06	+0.15	+0.27	+0.15	+0.08			
-30	+0.29	+0.23	+0.11	+0.08	+0.13	+0.29	+0.34	+0.25	+0.15			
-60	+0.23											
-90	0.00											

TABLE VI: RUN SCHEDULE

A. Rigid Model Tests, Model A in Aerolab Wind Tunnel

Test Run Number	Dynamic Pressure, (psf)	Pitch Angle	Yaw Angle	Comments
1	3.85 to 57.8 in increments of 4.0	0	0	C_D, C_L, C_M vs N_{RE}
2	"	-30	0	"
3	"	+30	0	"
4	"	0	30	"
5	"	-30	30	"
6	"	+30	30	"
7	"	0	60	"
8	"	-30	60	"
9	"	+30	60	"
10	"	0	90	"
11	"	-30	90	"
12	"	+30	90	"
13	"	0	120	"
14	"	-30	120	"
15	"	+30	120	"
16	"	-30	150	"
17	"	0	150	"
18	"	+30	150	"
19	"	0	180	"
20	"	-30	180	"

Test Run Number	Dynamic Pressure, (psf)	Pitch Angle	Yaw Angle	Comments
21	3.85 to 57.8 in increments of 4.0	+30	180	C_D, C_L, C_M vs N_{RE}
22	"	0	210	"
23	"	-30	210	"
24	"	+30	210	"
25	"	-30	240	"
26	"	0	240	"
27	"	+30	240	"
28	"	0	270	C_D vs N_{RE}
29	"	-30	270	"
30	"	+30	270	"
31	"	0	300	"
32	"	-30	300	"
33	"	+30	300	"
34	"	0	330	"
35	"	-30	330	"
36	"	+30	330	"
37	46.1	-30 to +30 in 5 increments	0	C_D, C_L, C_M vs α
38	3.85 to 57.8 in increments of 4.0	+90	0	C_D, C_L, C_M vs N_{RE}
39	46.1	+60 to +120 in 5 increments	0	C_D, C_L, C_M vs α
40	3.85 to 57.8 in increments Of 4.0	+60	180	C_D, C_L, C_M vs N_{RE}

Test Run Number	Dynamic Pressure, (psf)	Pitch Angle	Yaw Angle	Comments
41	3.85 to 57.8 in increments of 4.0	+60	0	C_D, C_L, C_M VS N_{RE}
42	"	+60	30	"
43	"	+60	210	"
44	34.62 to 46.1	+90	30	"
45	3.85 to 42.3 in increments of 4.0	+60	60	"
46	"	+60	240	"
47	30.8 to 38.5	+90	60	"
48	3.85 to 42.3	+60	90	"
49	3.85 to 38.5	+90	90	"
50	3.85 to 42.4 in increments of 4.0	+60	270	C_D, C_L, C_M VS N_{RE}
51	"	+60	120	"
52	"	+60	300	"
53	"	+60	150	"
54	"	+60	330	"
55	46.1	-120 to -60 in 5 increments	0	C_D, C_L, C_M VS α
56	3.85 to 46.1 in increments of 4.0	-60	180	C_D, C_L, C_M VS N_{RE}
57	"	-90	0	"
58	"	-60	0	"
59	"	-60	210	"

Test Run Number	Dynamic Pressure (psf)	Pitch Angle	Yaw Angle	Comments
60	46.1	0	345 to 015 in 5 increments	C_D, C_F, C_N vs ψ
61	"	"	020 to 045 in 5 increments	"
62	"	"	050 to 075 in 5 increments	"
63	"	"	080 to 105 in 5 increments	"
64	"	"	110 to 135 in 5 increments	"
65	"	"	140 to 165 in 5 increments	"
66	"	"	170 to 195 in 5 increments	"
67	"	"	200 to 225 in 5 increments	"
68	"	"	230 to 255 in 5 increments	"
69	"	"	260 to 285 in 5 increments	"
70	"	"	290 to 315 in 5 increments	"
71	"	"	320 to 340 in 5 increments	"

B. Dynamic Model Tests, West Coast Research Wind Tunnel

Test Run No.	Model Used	Dynamic Pressure,	Photographs (Motion Picture)	Time-History Trace
Not Numbered (Note 1)	B	0.5 to 1.0 psf	none	none
M-1 - M-15 (Note 2)	C	5.0	yes	none
1 - 9 (Note 3)	C	5.0	no	yes
10, 11	C	2.5	no	yes
12	C	7.5	no	yes
13, 14	C	2.0	no	yes
15, 16	C	3.0	no	yes
17, 18	C	4.0	no	yes
19, 20	C	5.0	no	yes
21, 22	C	6.0	no	yes
23	C	7.0	no	yes
24, 25	C	8.0	no	yes
24A (Note 4)	C	2.0	yes film test sequency 16	yes (note 5)
25A	C	3.0	yes film test sequence 17	yes
26	C	4.0	yes film test sequence 18	yes
27	C	5.0	yes	yes

Test Run No.	Model Used	Dynamic Pressure,	Photographs (Motion Picture)	Time-History Trace
28	C	5.0	yes film test sequence 19	yes
29	C	6.0	yes film test sequence 20	yes
30	C	7.0	yes film test sequence 21	yes
31	C	7.0	yes film test sequence 22	yes
32	C	8.0	yes film test sequence 23	yes
33	C	8.0	yes	yes
L-1, L-2, L-3	D	2.0	no	yes
L-4, L-5	D	3.0	no	yes
L-6, L-7	D	4.0	no	yes
L-8, L-9	D	5.0	no	yes
L-10, L-11 L-12	D	6.0	no	yes
L-13, L-14	D	7.0	no	yes
L-15, L-16 L-17, L-18	D	8.0	no	yes
LL-1, LL-2	E	2.0	no	yes
LL-3, LL-4	E	3.0	no	yes
LL-5, LL-6	E	4.0	no	yes
LL-7, LL-8 LL-9	E	5.0	no	yes

Test Run No.	Model Used	Dynamic Pressure,	Photographs (Motion Picture)	Time-History Trace
LL-10, LL-11	E	6.0	no	yes
LL-12, LL-13 LL-14, LL-15	E	7.0	no	yes
LL-16, LL-17	E	8.0	no	yes

Notes:

1. Various runs conducted in both the Aerolab tunnel and the West Coast Research tunnel. Model mounted on wire in order to observe both the yaw mode and the pitch mode.
2. Local tie down constraints not used; these runs correspond to Part One of the movie film. Film test sequences 1 through 15; film speed, 16 frames per second.
3. Local tie down constraints were used in this and subsequent runs listed.
4. Runs 24A through 33 correspond to Part Two of the movie film. Film test sequences 16 through 23; film speed, 16 frames per second.
5. Test run numbers (24A through 33, L-1 through L-18, LL-1 through LL-17) correspond with notation used on the time-history traces.

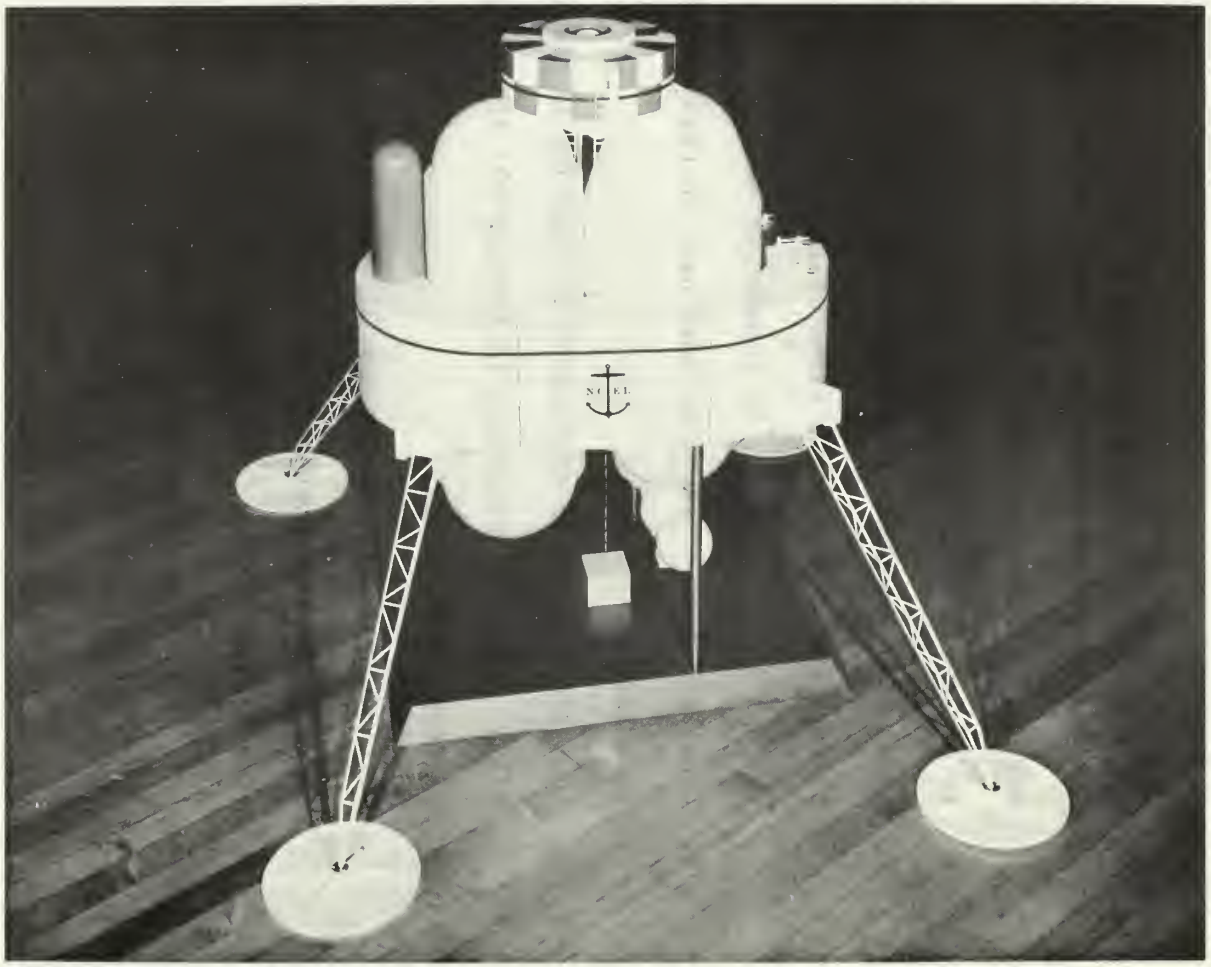

OFFICIAL U. S. NAVY PHOTOGRAPH (LDH)
PORT HUENEME, CALIFORNIA

4846- 5-68

FIG 1 MOCK-UP OF THE MANNED UNDERWATER STATION

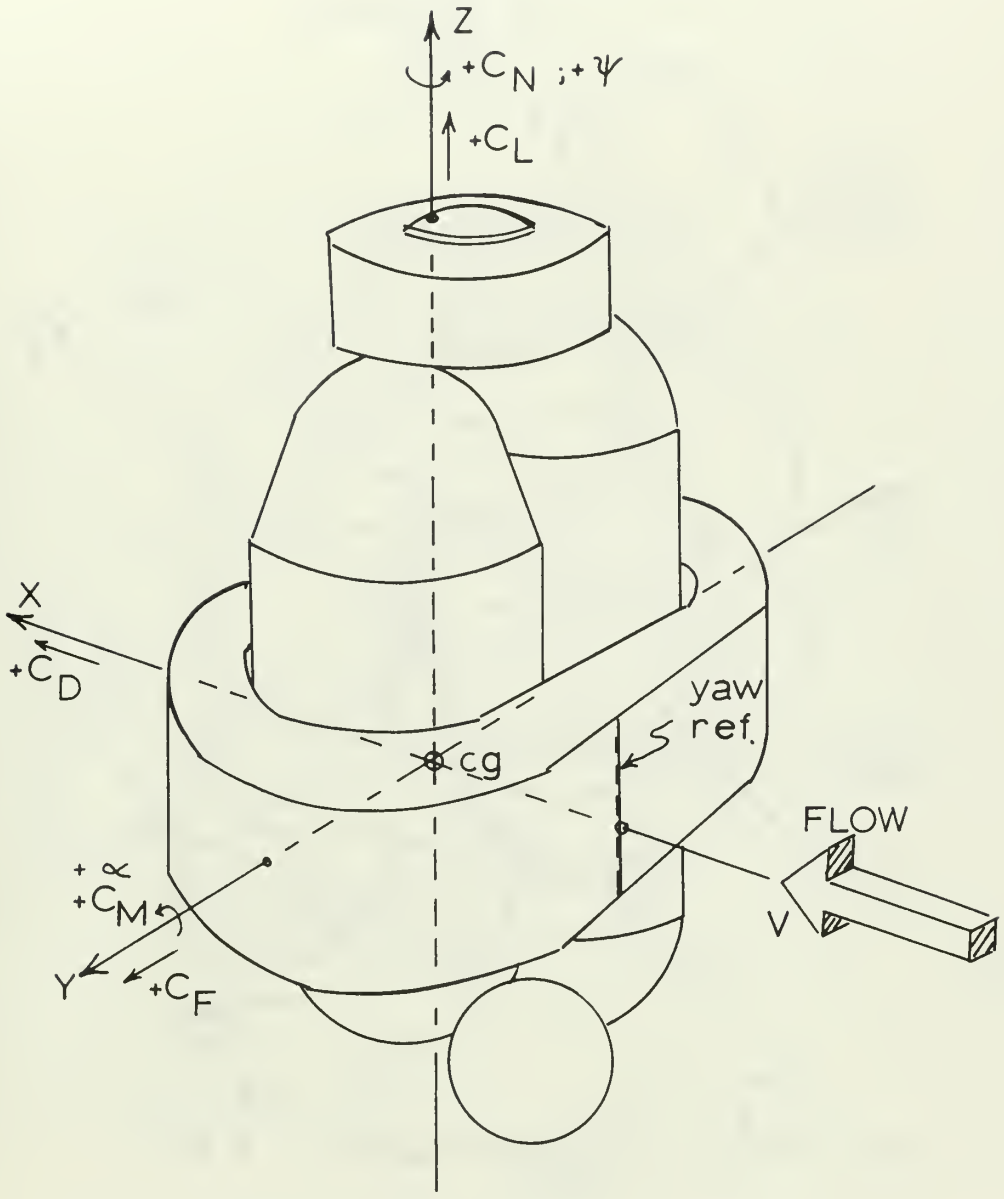

1. MODEL SHOWN AT ZERO PITCH AND ZERO YAW.
2. FORCES AND MOMENTS ARE RELATIVE TO WIND AXIS SYSTEM (AS ABOVE).

FIG. 2 COORDINATE AXIS SYSTEM

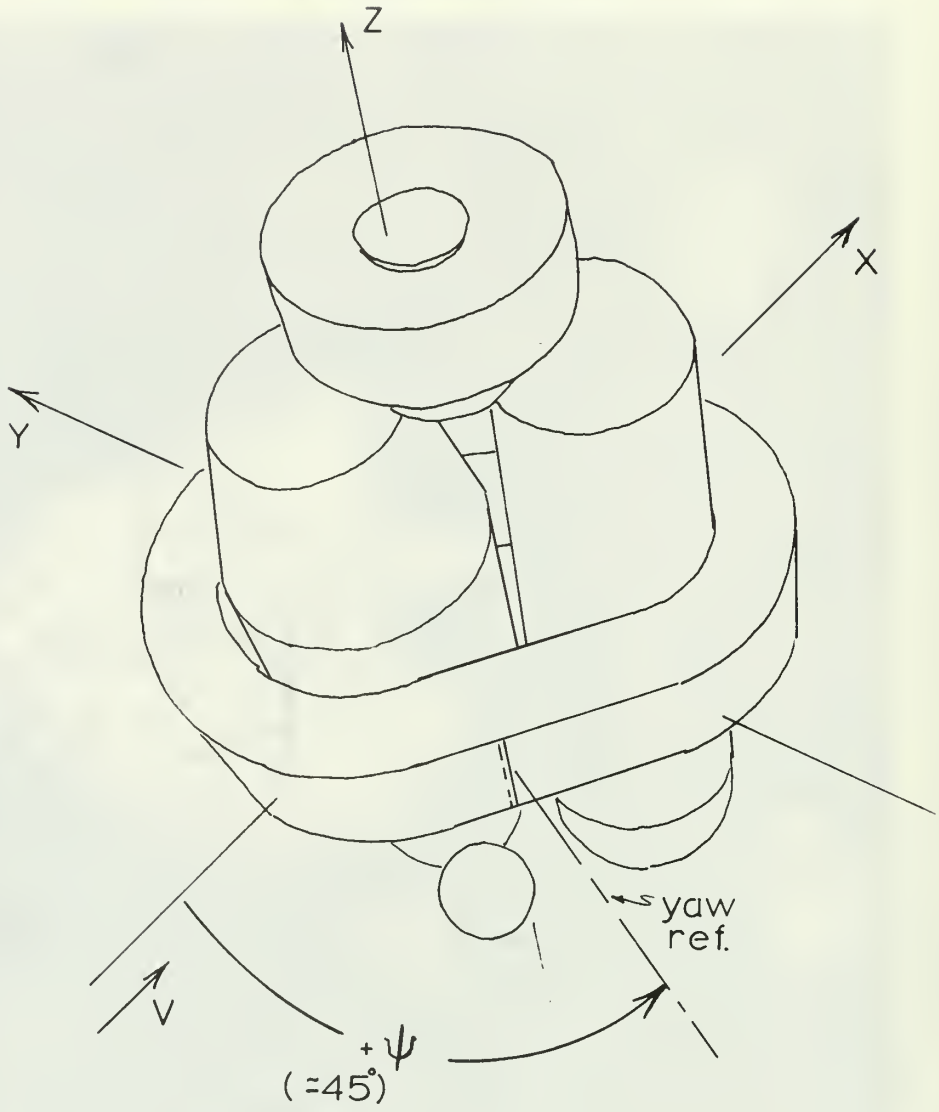

FIG. 3 YAW ANGLE DEFINITION

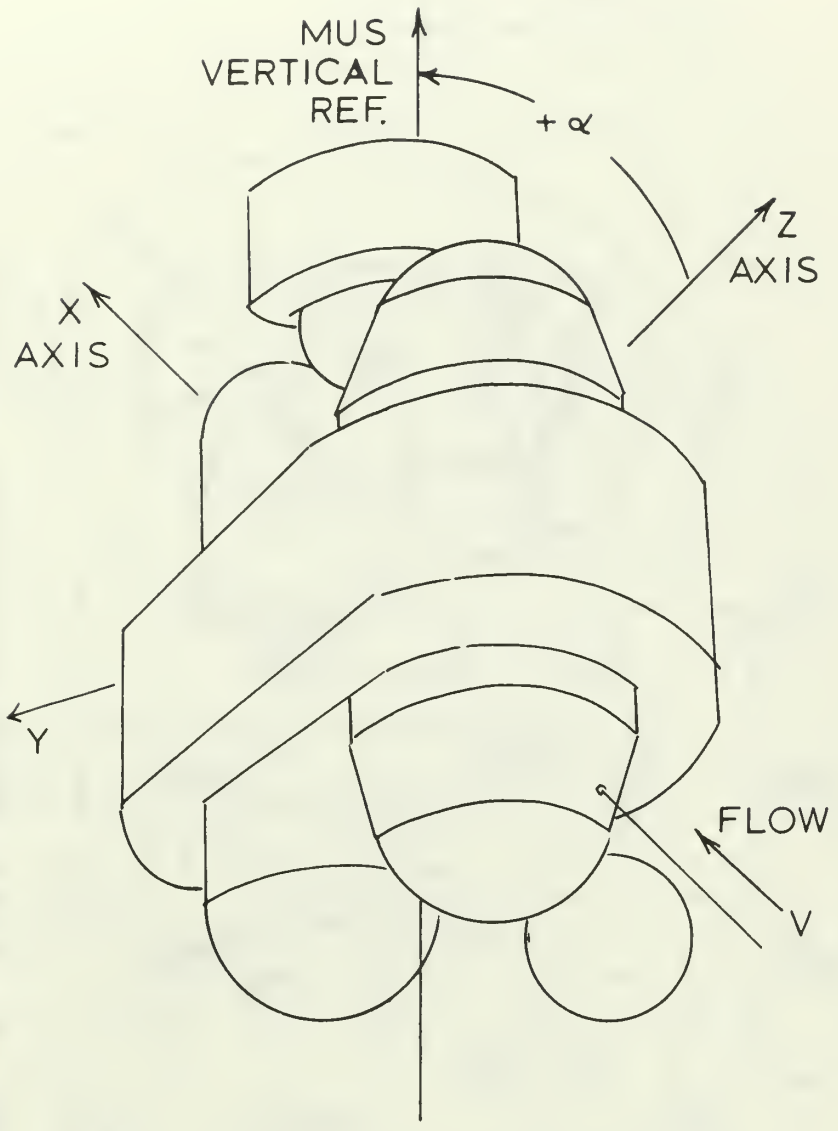

FIG. 4 PITCH ANGLE DEFINITION

FIG. 5
EXTERIOR DIMENSIONS
OF THE MUS MODEL

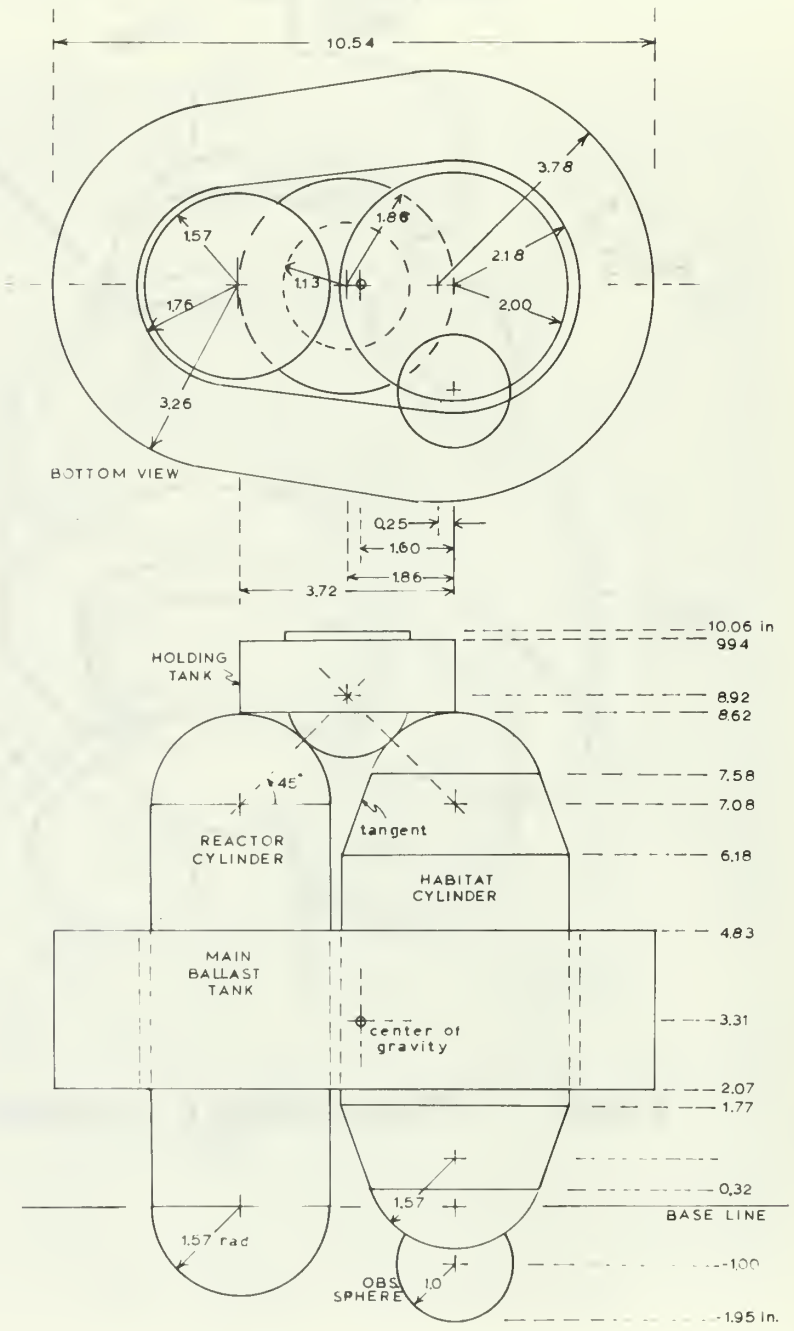

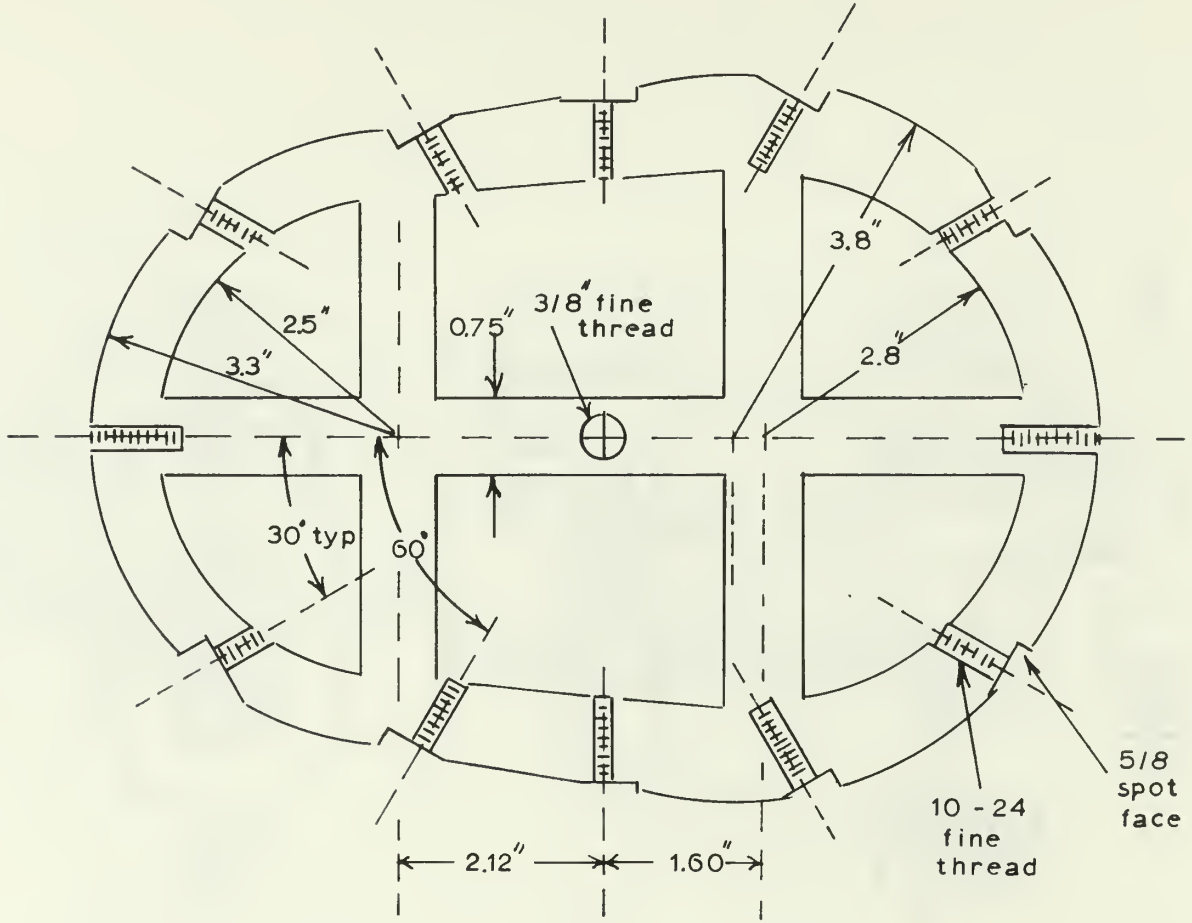

FIG. 6 ALUMINUM SPAR USED IN THE RIGID MODEL

FIG. 7
WEIGHT DISTRIBUTION
IN THE DYNAMIC MODEL

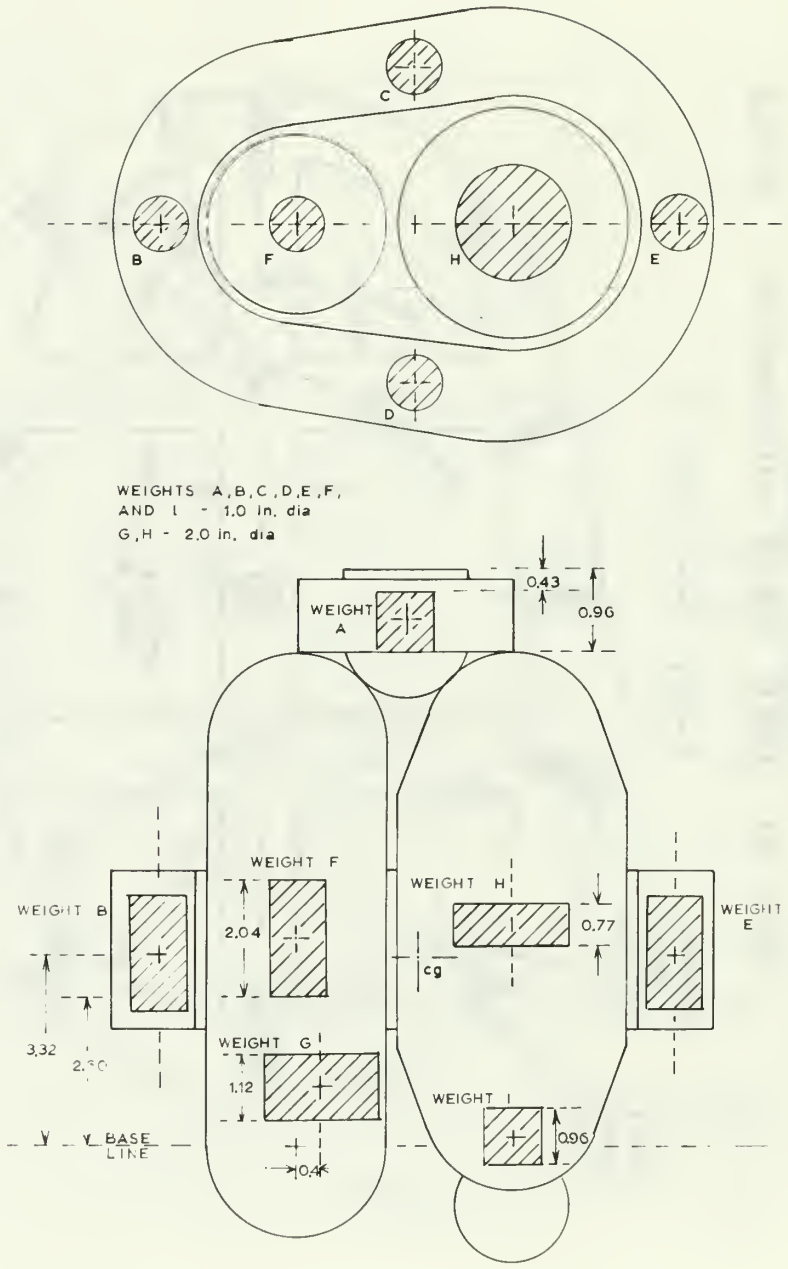

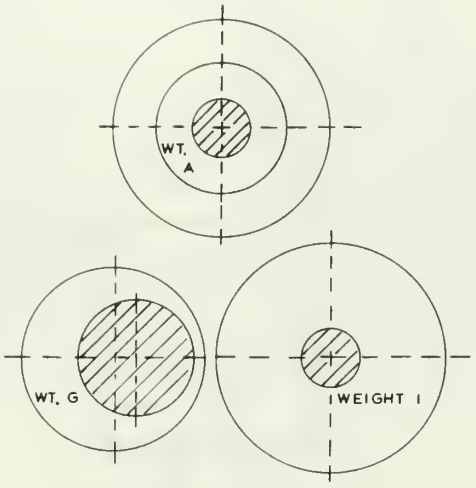

COMPONENT	WEIGHT	DIA.	HEIGHT
WEIGHT A	0.30 lbs	1.0	0.96
WEIGHT B	0.67 lbs	1.0	2.07
WEIGHT C	0.67 lbs	1.0	2.07
WEIGHT D	0.67 lbs	1.0	2.07
WEIGHT E	0.67 lbs	1.0	2.07
WEIGHT F	0.67 lbs	1.0	2.04
WEIGHT G	1.45 lbs	2.0	1.12
WEIGHT H	1.00 lbs	2.0	0.77
WEIGHT I	0.31 lbs	1.0	0.96
HOLDING TANK	0.20 lbs		
REACTOR CYLINDER	0.74 lbs		
HABITAT CYLINDER	0.80 lbs		
MAIN BALLAST TANK	1.25 lbs		
OBSERVATION SPHERE	0.05 lbs		

FIG. 8

WEIGHT DISTRIBUTION
IN THE DYNAMIC MODEL

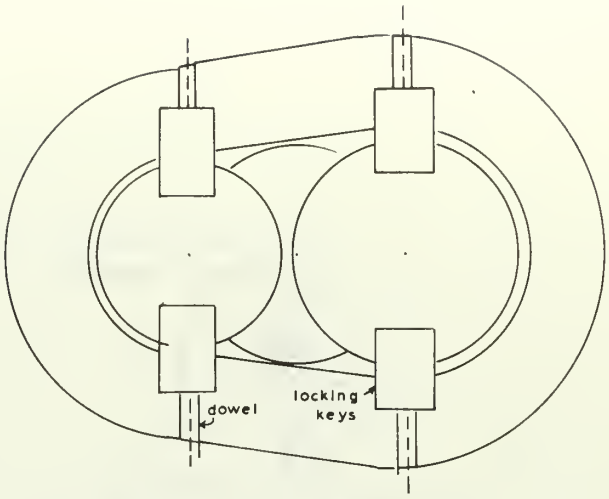

FIG 9

FASTENING METHOD FOR THE DYNAMIC MUS MODEL

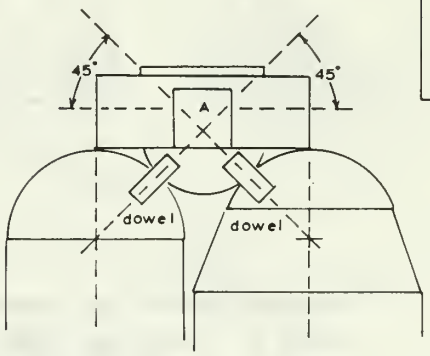

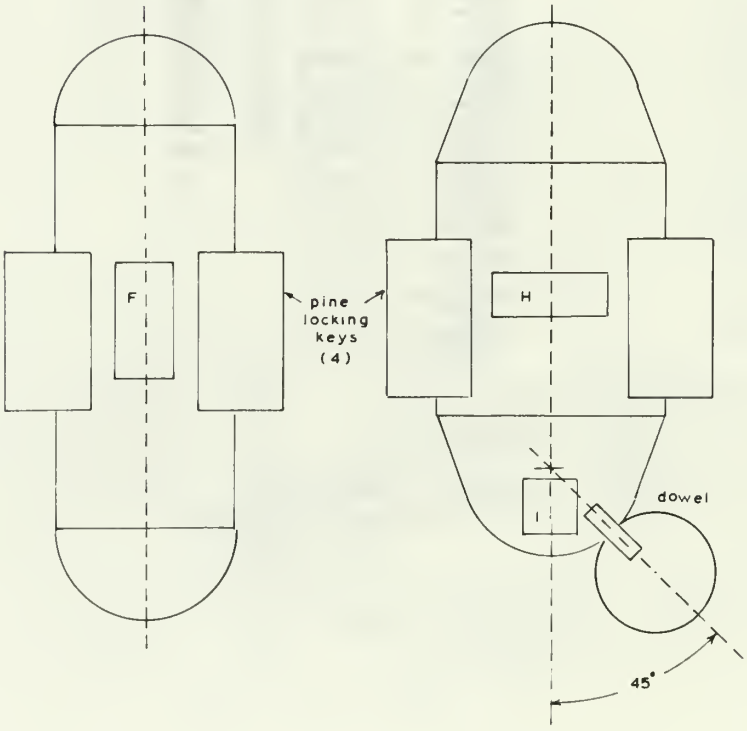

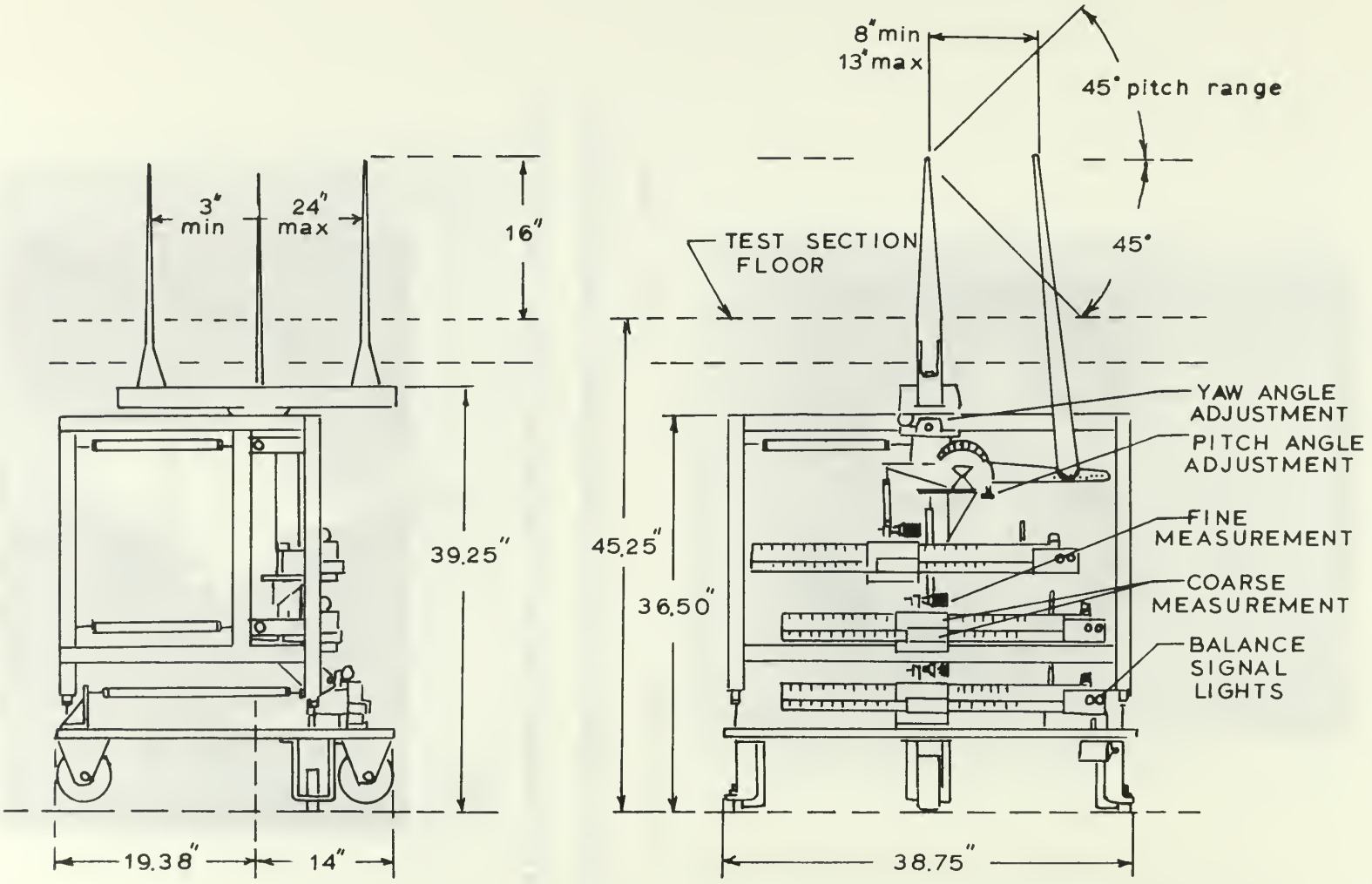

FIG. 10 THE AEROLAB 3 COMPONENT BEAM BALANCE

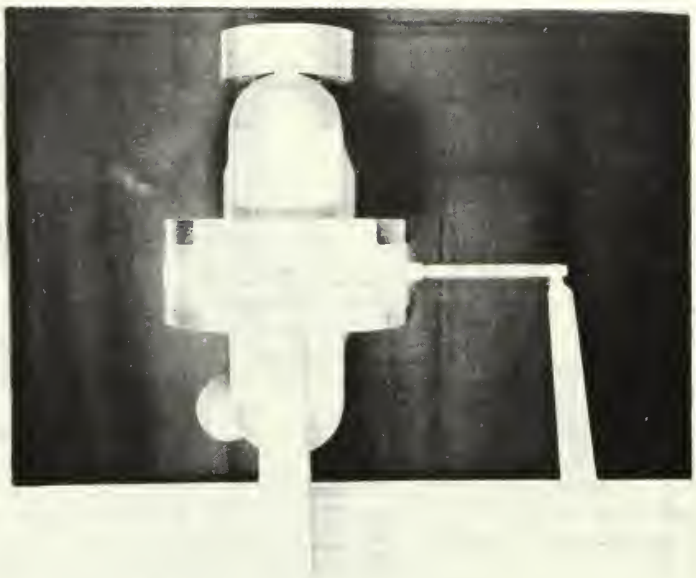

Fig. 11 - Model orientation: yaw zero degrees, pitch zero degrees; viewed from left side of model; airflow left to right

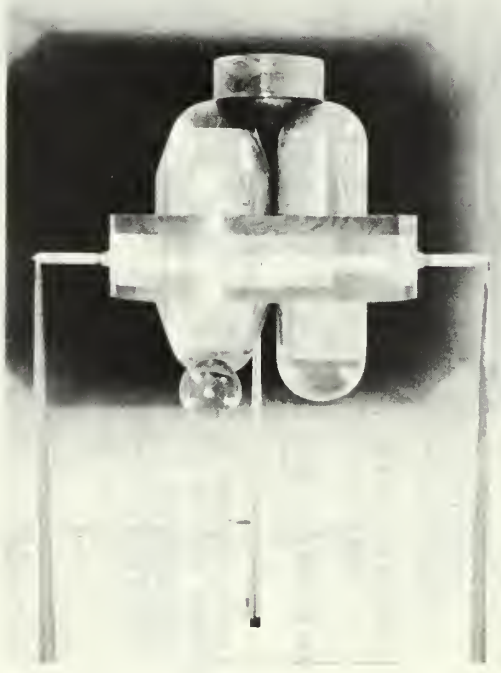

Fig. 12 - Model orientation: yaw zero degrees, pitch zero degrees; viewed from upstream side

Fig. 13 - Model orientation: yaw zero degrees, pitch +30 degrees; viewed from left side of model; airflow left to right

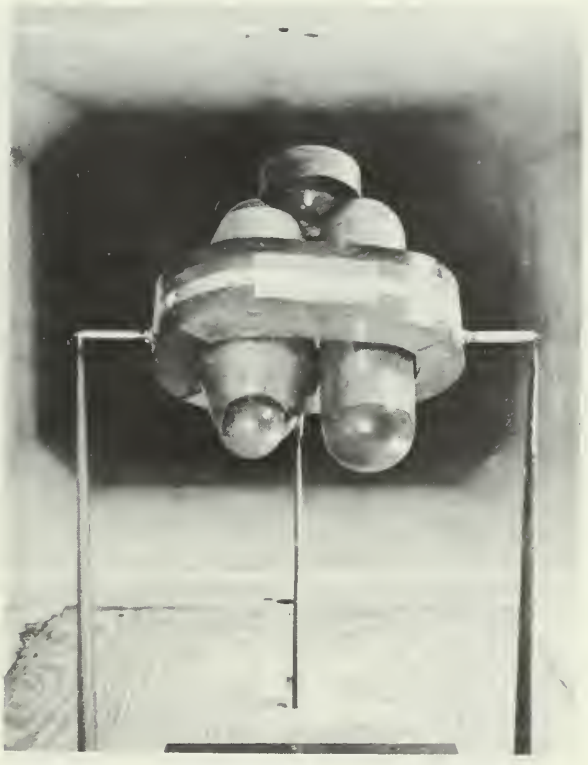

Fig. 14 - Model orientation: yaw zero degrees, pitch +30 degrees; viewed from upstream side

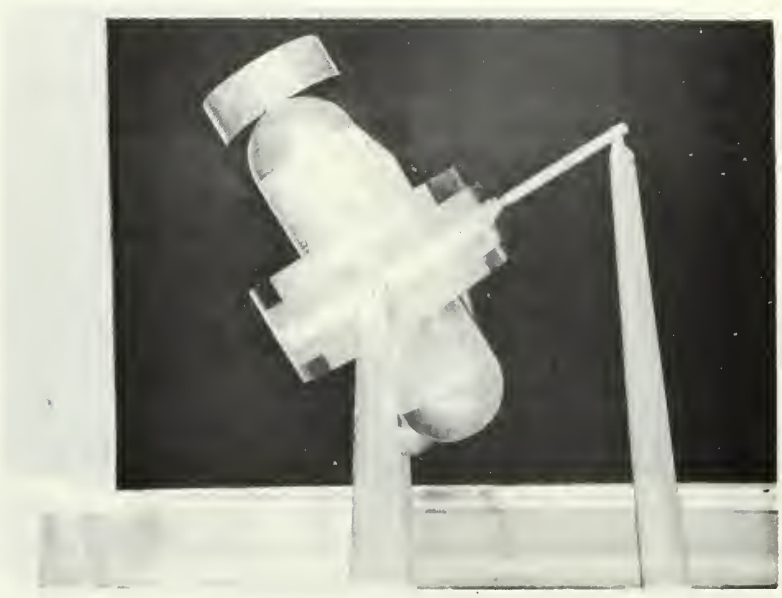

Fig. 15 - Model orientation: yaw zero degrees, pitch -30 degrees; viewed from left side of model; airflow left to right

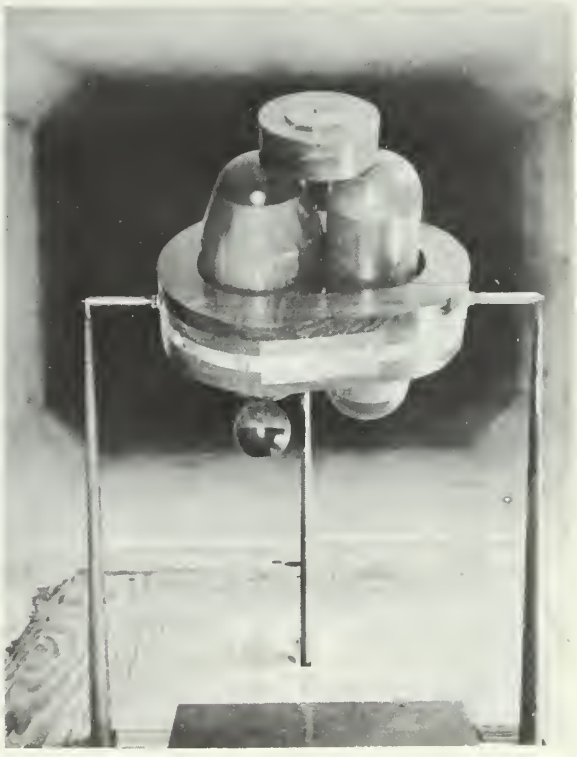

Fig. 16 - Model orientation: yaw zero degrees, pitch -30 degrees; viewed from upstream side

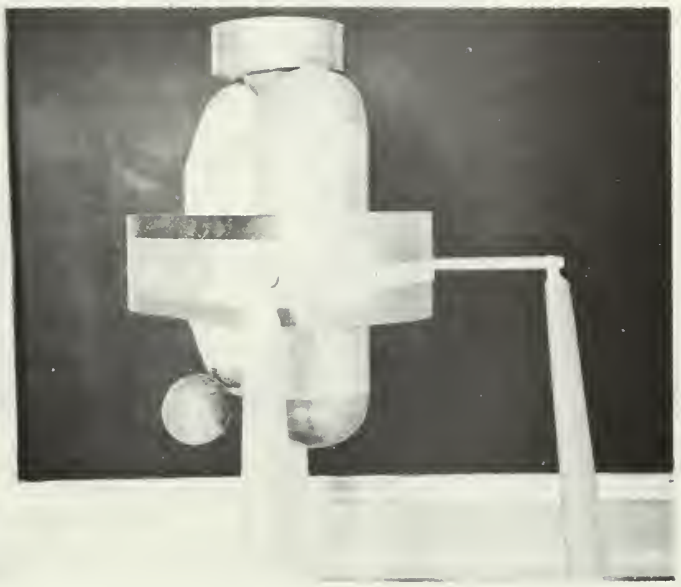

Fig. 17 - Model orientation: yaw 30 degrees, pitch zero degrees; viewed from left side of model; airflow left to right

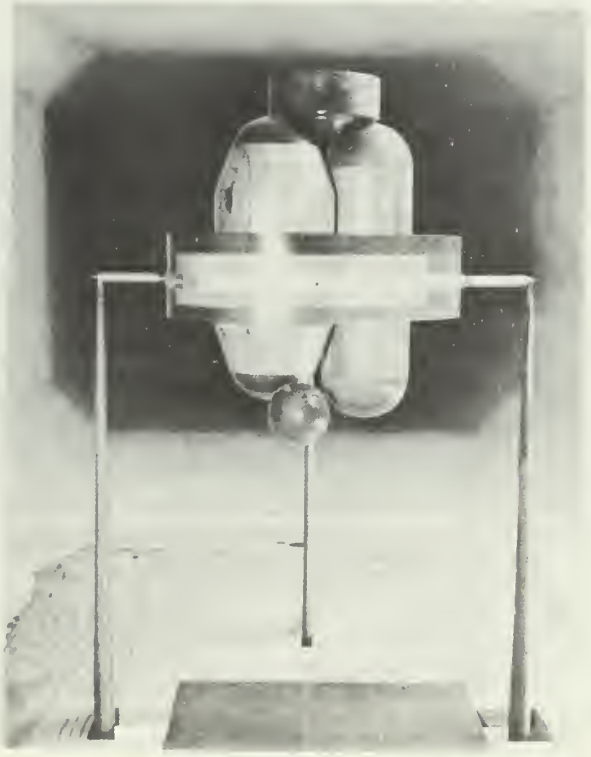

Fig. 18 - Model orientation: yaw 30 degrees, pitch zero degrees; viewed from upstream side

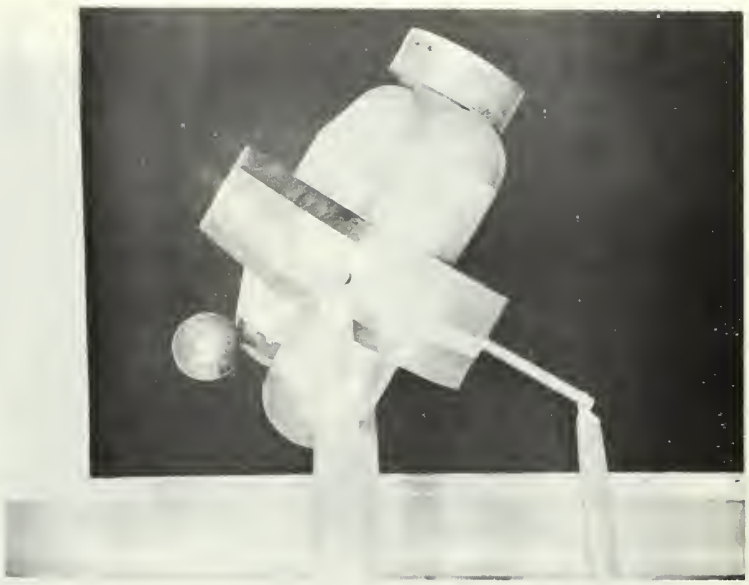

Fig. 19 - Model orientation: yaw 30 degrees, pitch +30 degrees; viewed from left side of model; airflow left to right

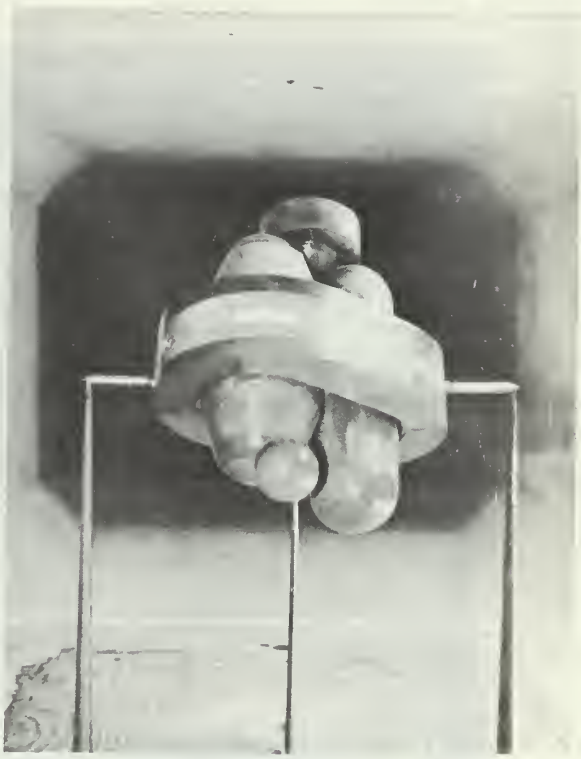

Fig. 20 - Model orientation: yaw 30 degrees, pitch +30 degrees; viewed from upstream side

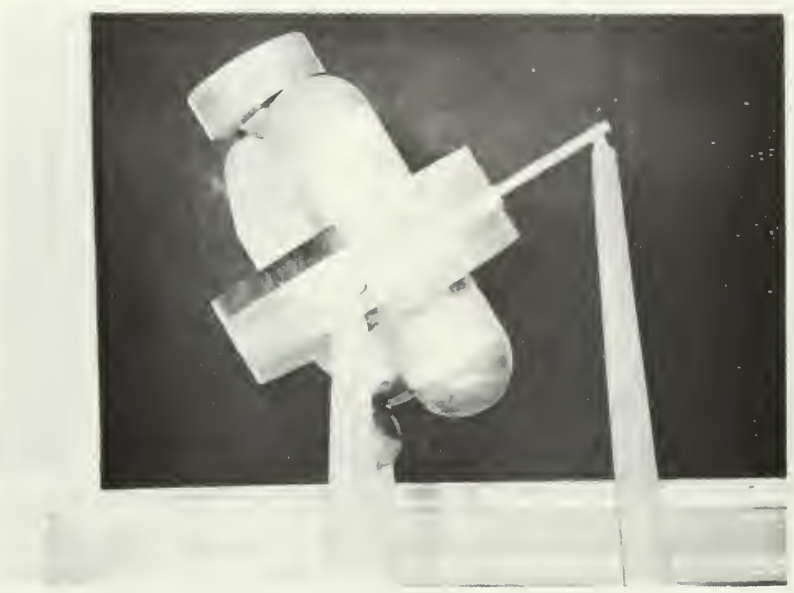

Fig. 21 - Model orientation: yaw 30 degrees; pitch -30 degrees; viewed from left side of model; airflow left to right

Fig. 22 - Model orientation: yaw 30 degrees, pitch -30 degrees; viewed from upstream side

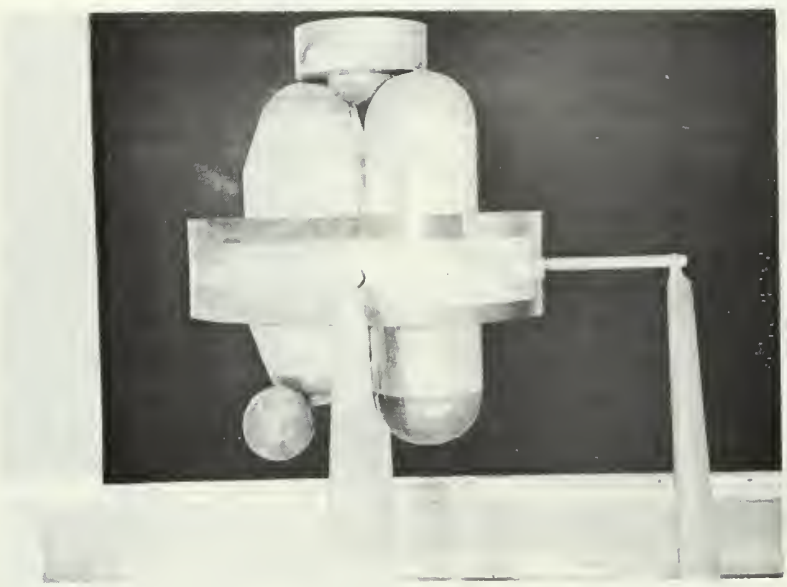

Fig. 23 - Model orientation: yaw 60 degrees, pitch zero degrees; viewed from left side of model; airflow left to right

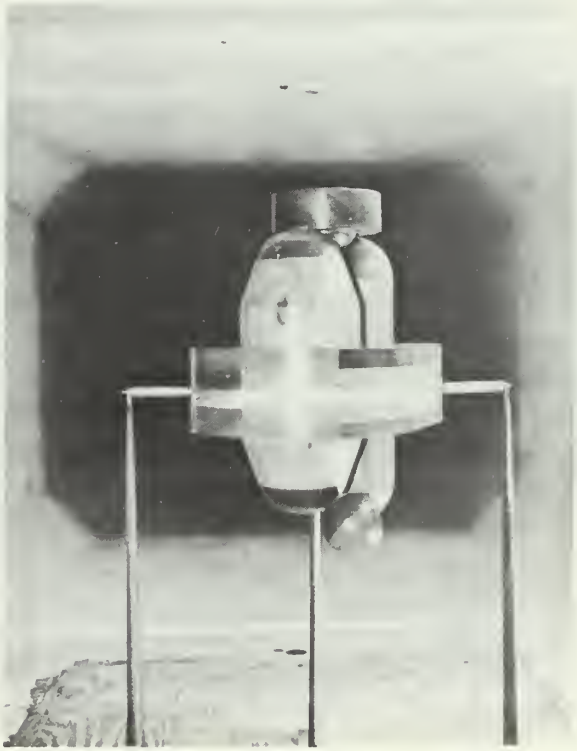

Fig. 24 - Model orientation: yaw 60 degrees, pitch zero degrees; viewed from upstream side

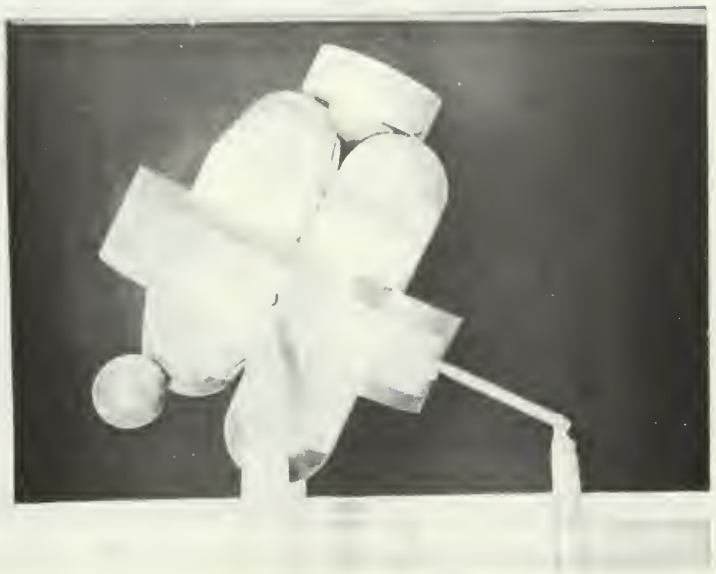

Fig. 25 - Model orientation: yaw 60 degrees, pitch +30 degrees; viewed from left side of model; airflow left to right

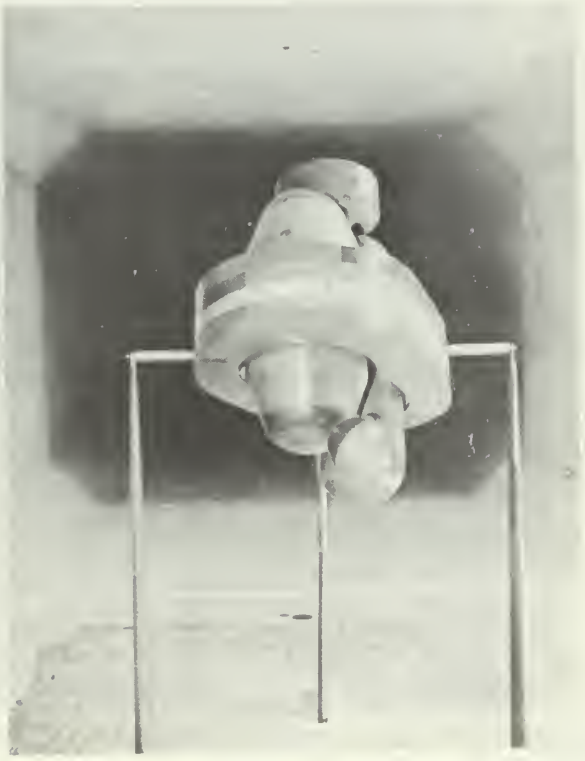

Fig. 26 - Model orientation: yaw 60 degrees, pitch +30 degrees; viewed from upstream side

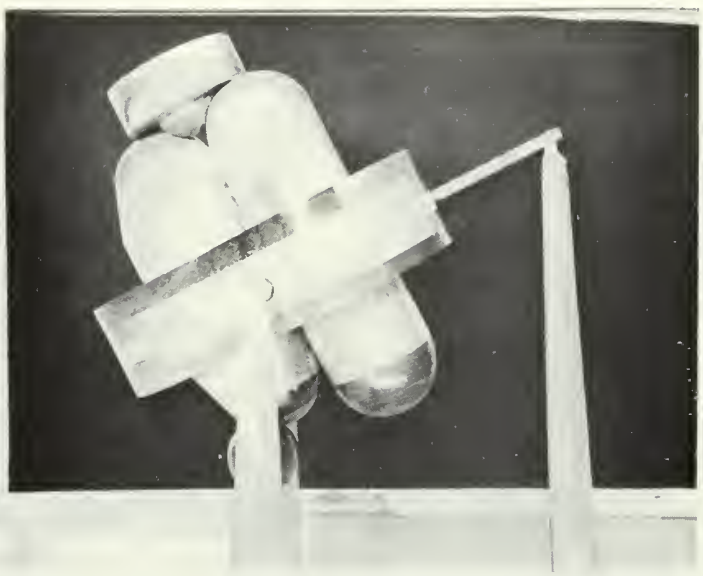

Fig. 27 - Model orientation: yaw 60 degrees; pitch -30 degrees; viewed from left side of model; airflow left to right

Fig. 28 - Model orientation: yaw 60 degrees, pitch -30 degrees; viewed from upstream side

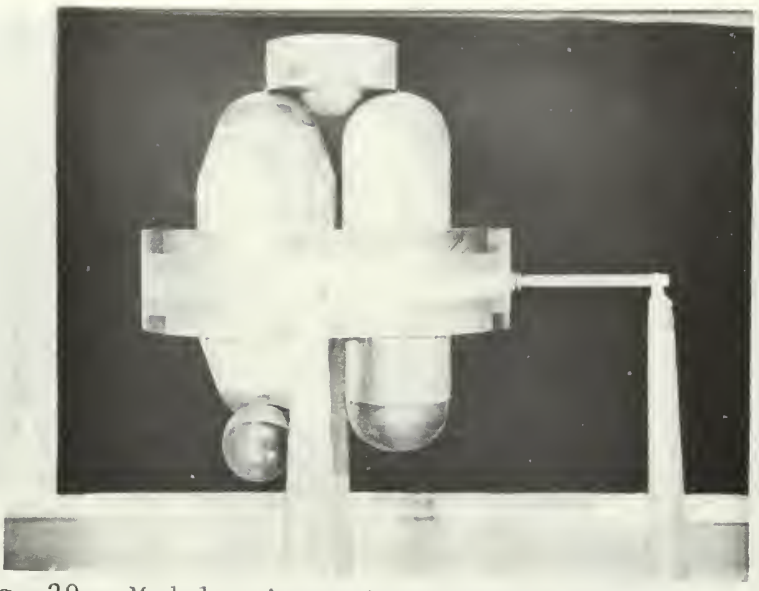

Fig. 29 - Model orientation: yaw 90 degrees, pitch zero degrees; viewed from left side of model; airflow left to right

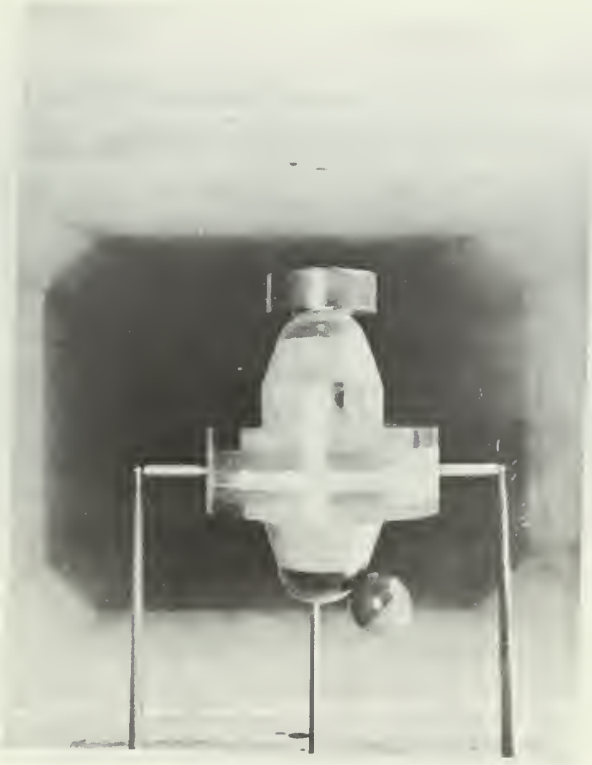

Fig. 30 - Model orientation; yaw 90 degrees, pitch zero degrees; viewed from upstream side

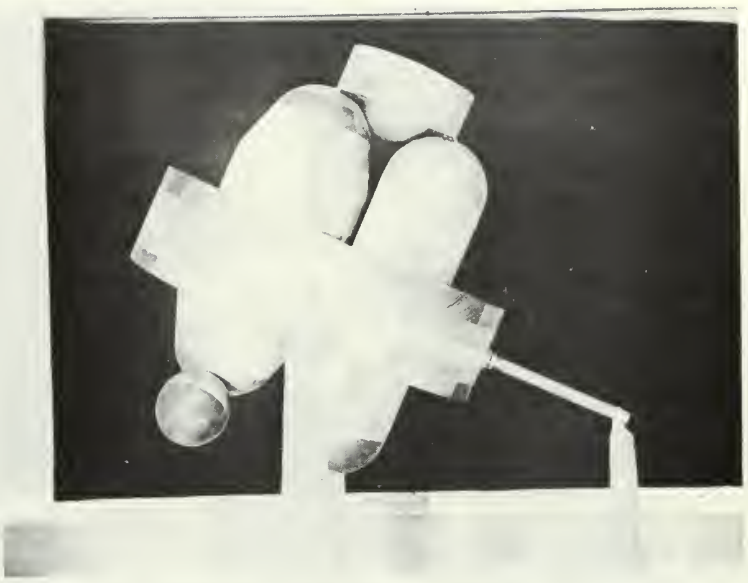

Fig. 31 - Model orientation: yaw 90 degrees, pitch +30 degrees; viewed from left side of model; airflow left to right

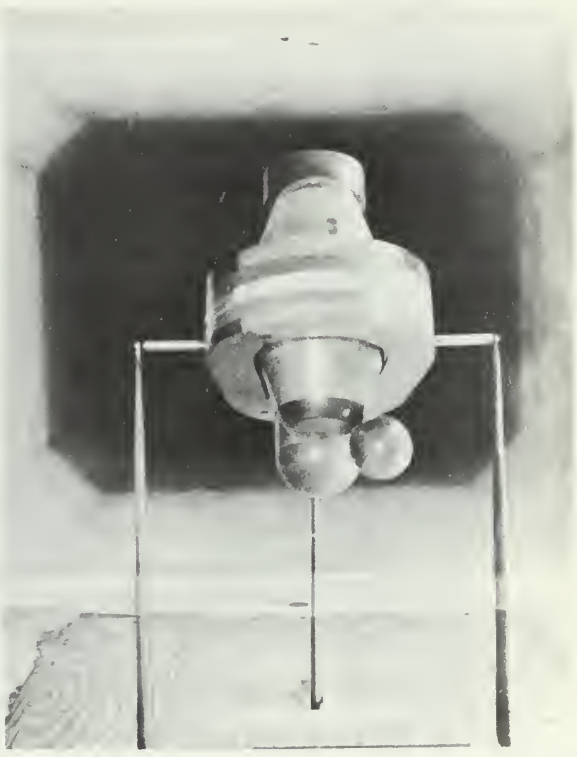

Fig. 32 - Model orientation: yaw 90 degrees, pitch +30 degrees; viewed from upstream side

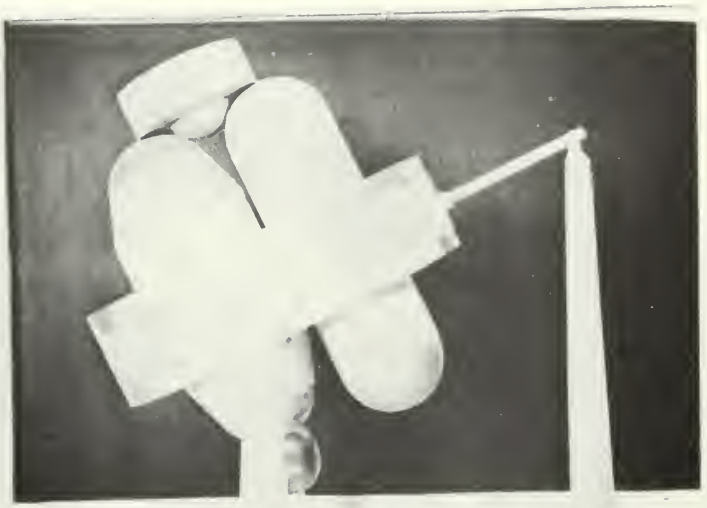

Fig. 33 - Model orientation: yaw 90 degrees, pitch -30 degrees; viewed from left side of model; airflow left to right

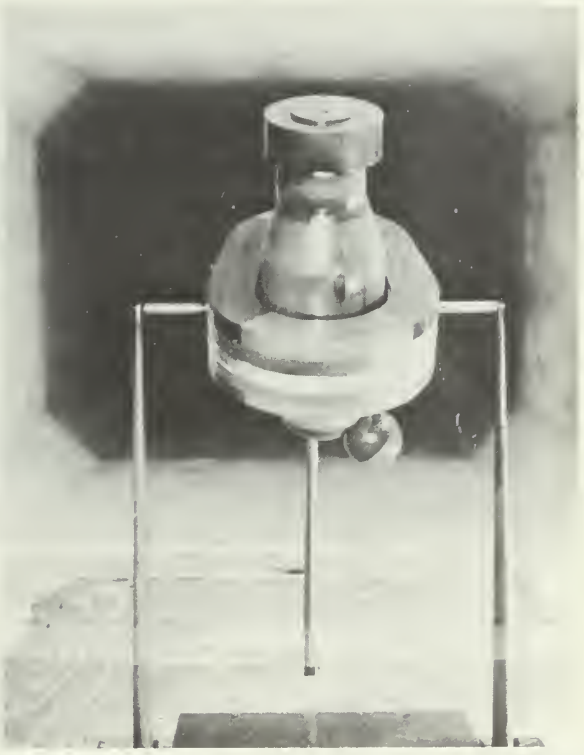

Fig. 34 - Model orientation: yaw 90 degrees, pitch -30 degrees; viewed from upstream side

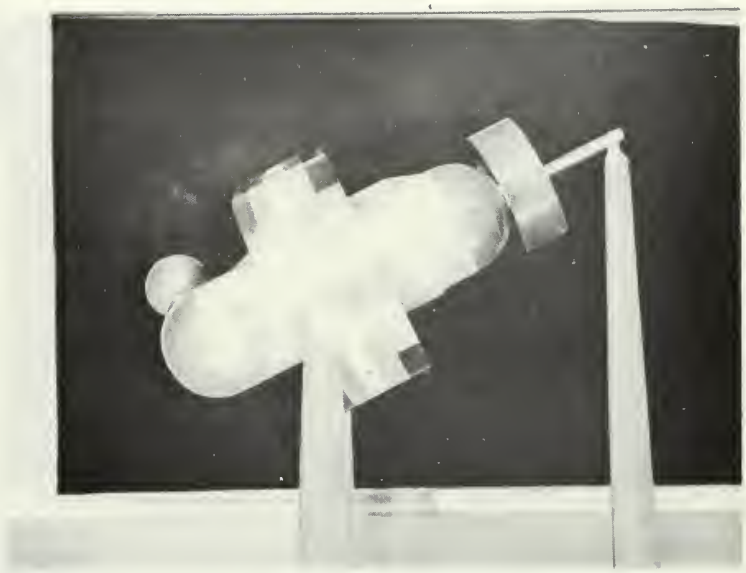

Fig. 35 - Model orientation: yaw zero degrees, pitch +60 degrees; viewed from left side of model; airflow left to right

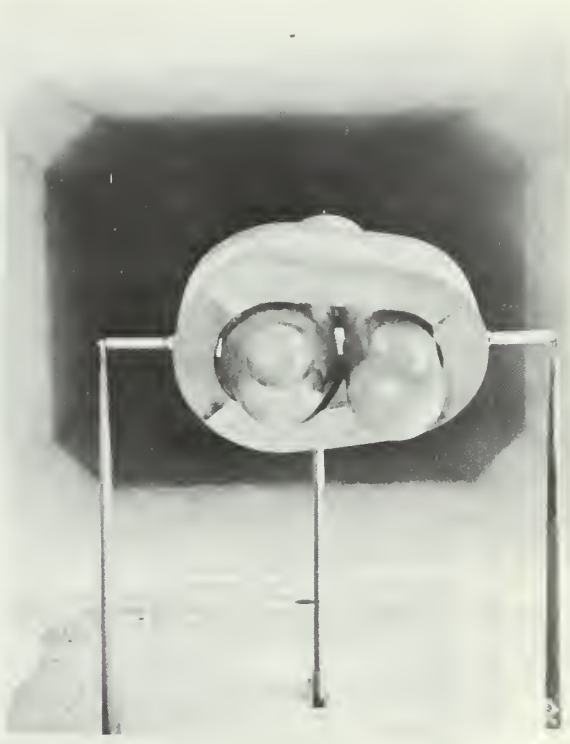

Fig. 36 - Model orientation: yaw zero degrees, pitch +60 degrees; viewed from upstream side

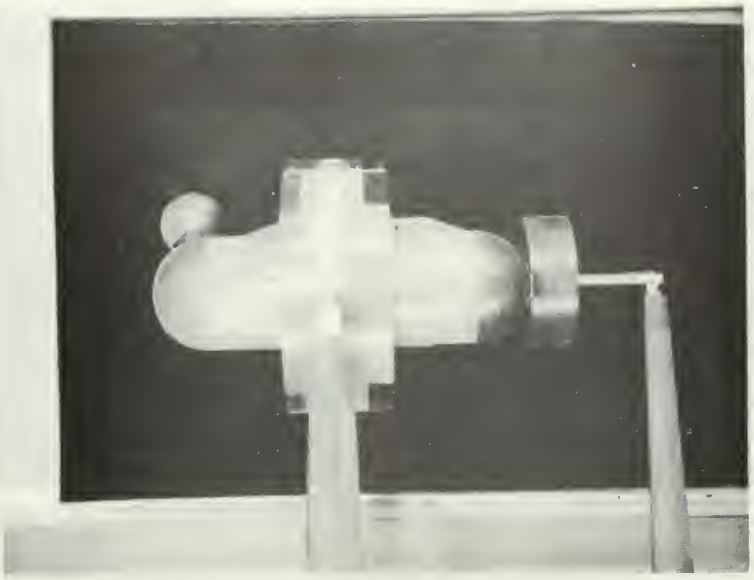

Fig. 37 - Model orientation: yaw zero degrees, pitch +90 degrees; viewed from left side of model; airflow left to right

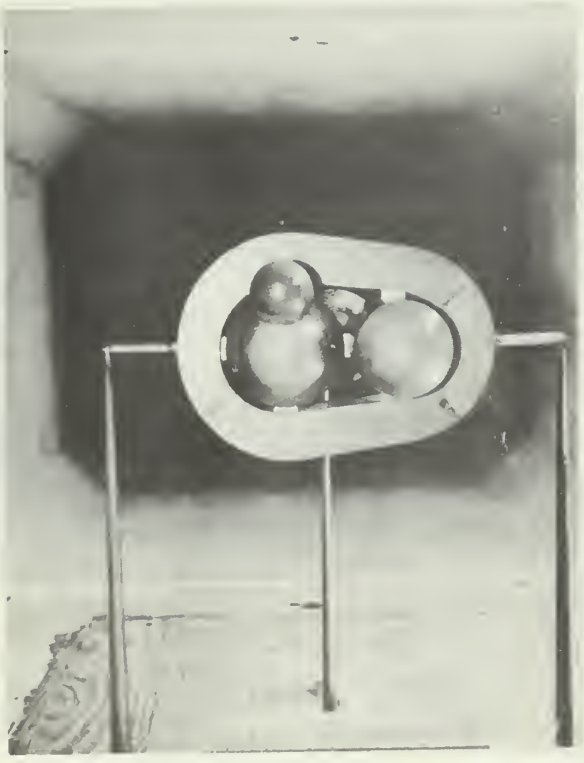

Fig. 38 - Model orientation: yaw zero degrees, pitch +90 degrees; viewed from upstream side

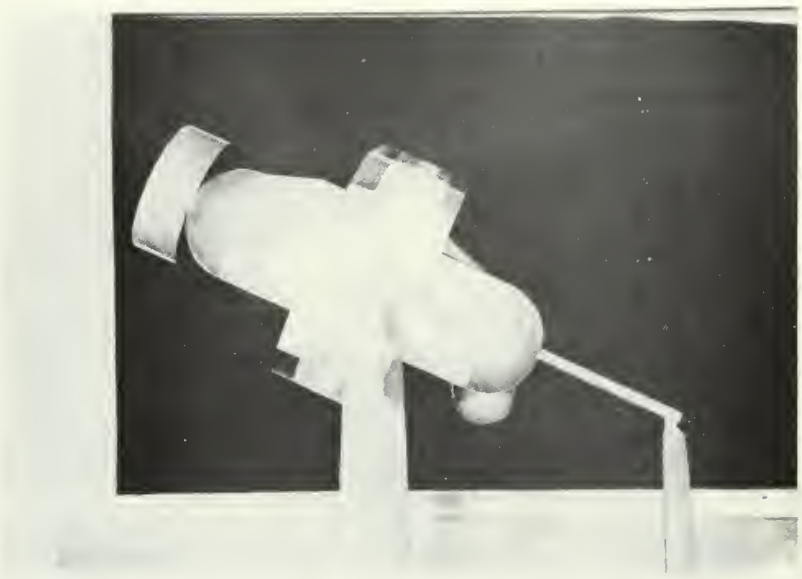

Fig. 39 - Model orientation: yaw zero degrees, pitch -60 degrees; viewed from left side of model; airflow left to right

Fig. 40 - Model orientation: yaw zero degrees, pitch -60 degrees; viewed from upstream side

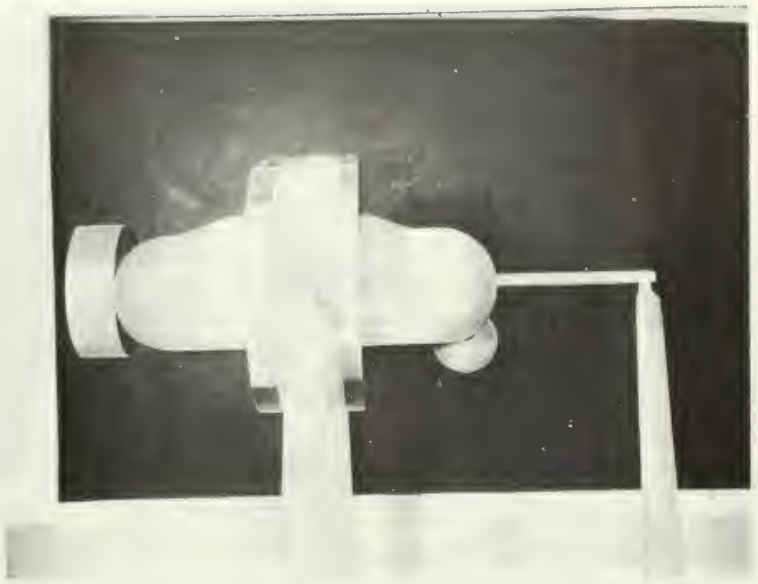

Fig. 41 - Model orientation: yaw zero degrees, pitch -90 degrees; viewed from left side of model; airflow left to right

Fig. 42 - Model orientation: yaw zero degrees, pitch -90 degrees; viewed from upstream side

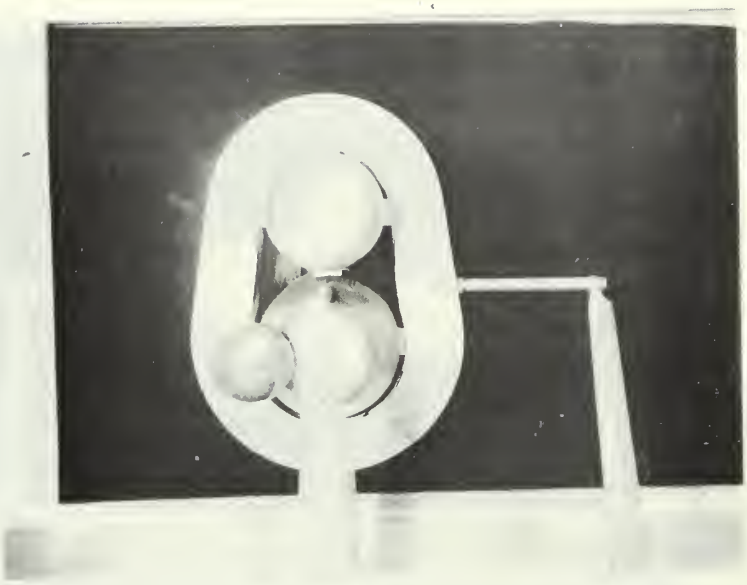

Fig. 43 - Support arrangement used for yaw variation in five degree increments; model at zero degrees pitch; viewed from side; flow left to right

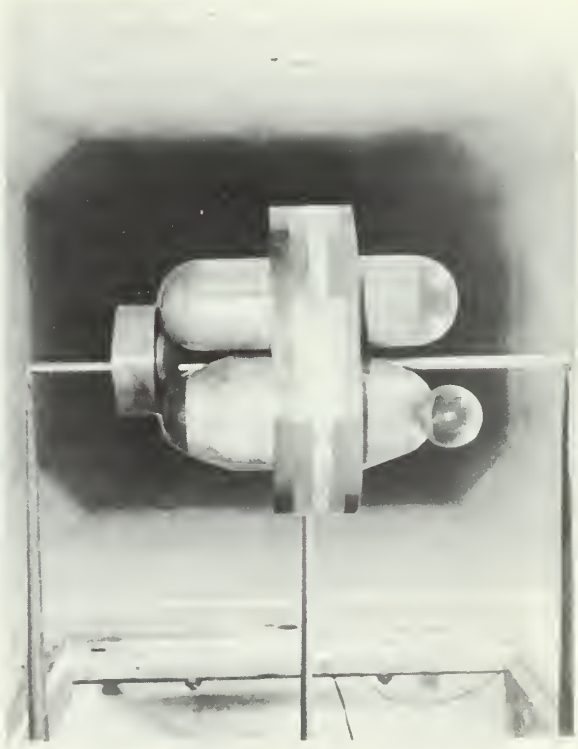

Fig. 44 - Same as 43, but view from upstream side

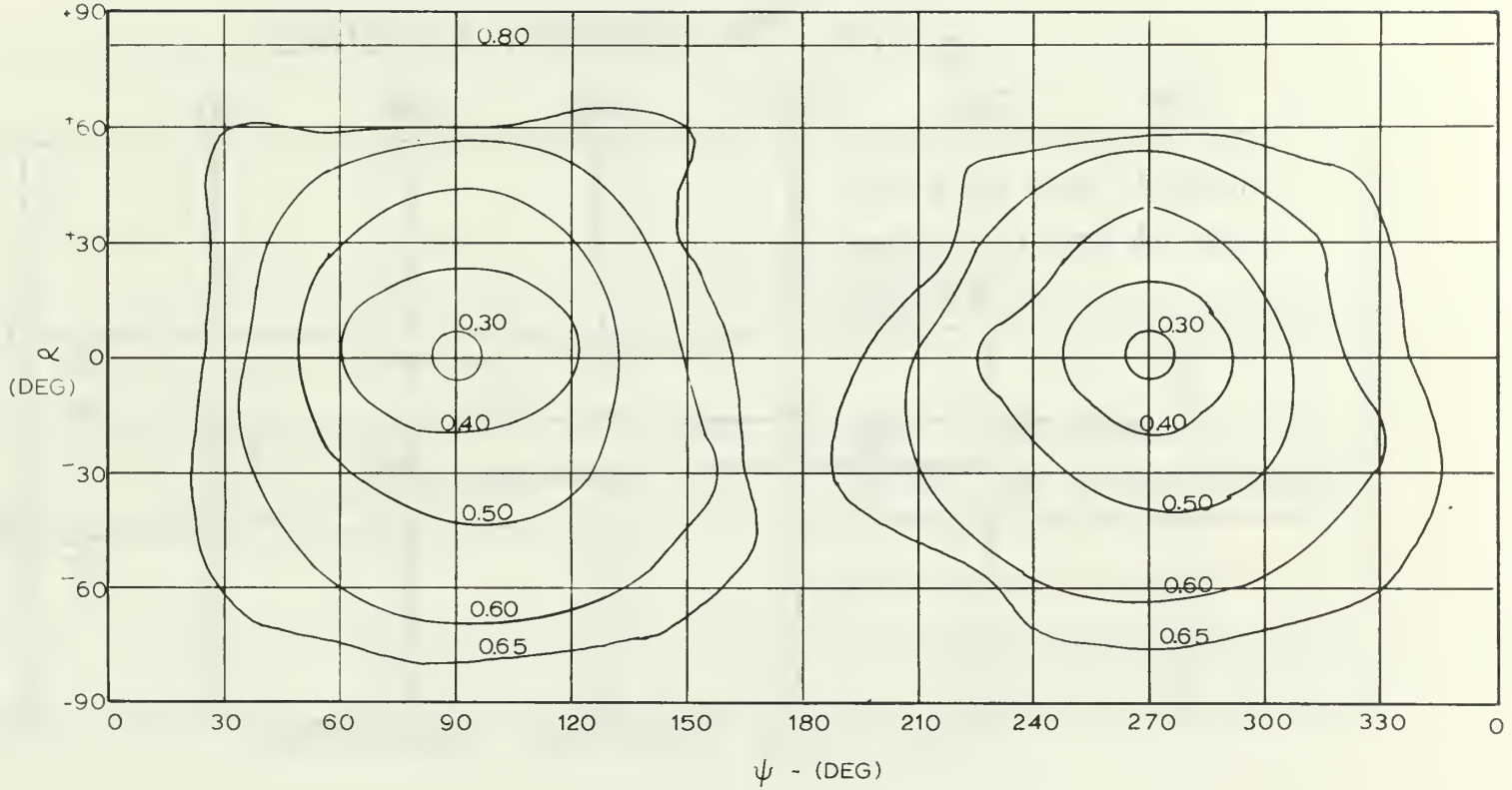

FIG. 45 DRAG SUMMARY CONTOUR PLOT

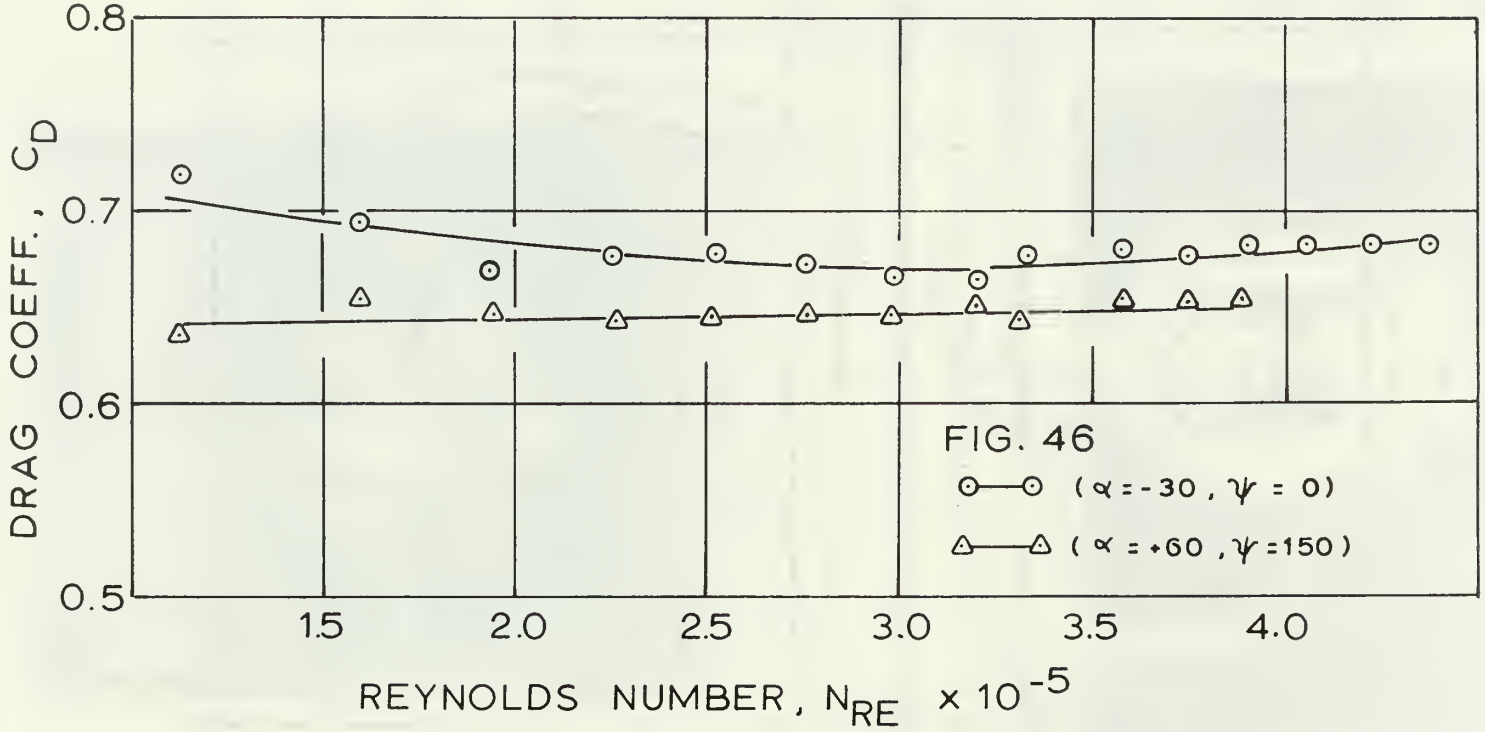
0.8
0.7
0.6
0.5
DRAG COEFF., C_D
1.5
2.0
2.5
3.0
3.5
4.0
REYNOLDS NUMBER, N_{RE} x 10^{-5}
FIG. 46
(α = -30, ψ = 0)
(α = +60, ψ = 150)

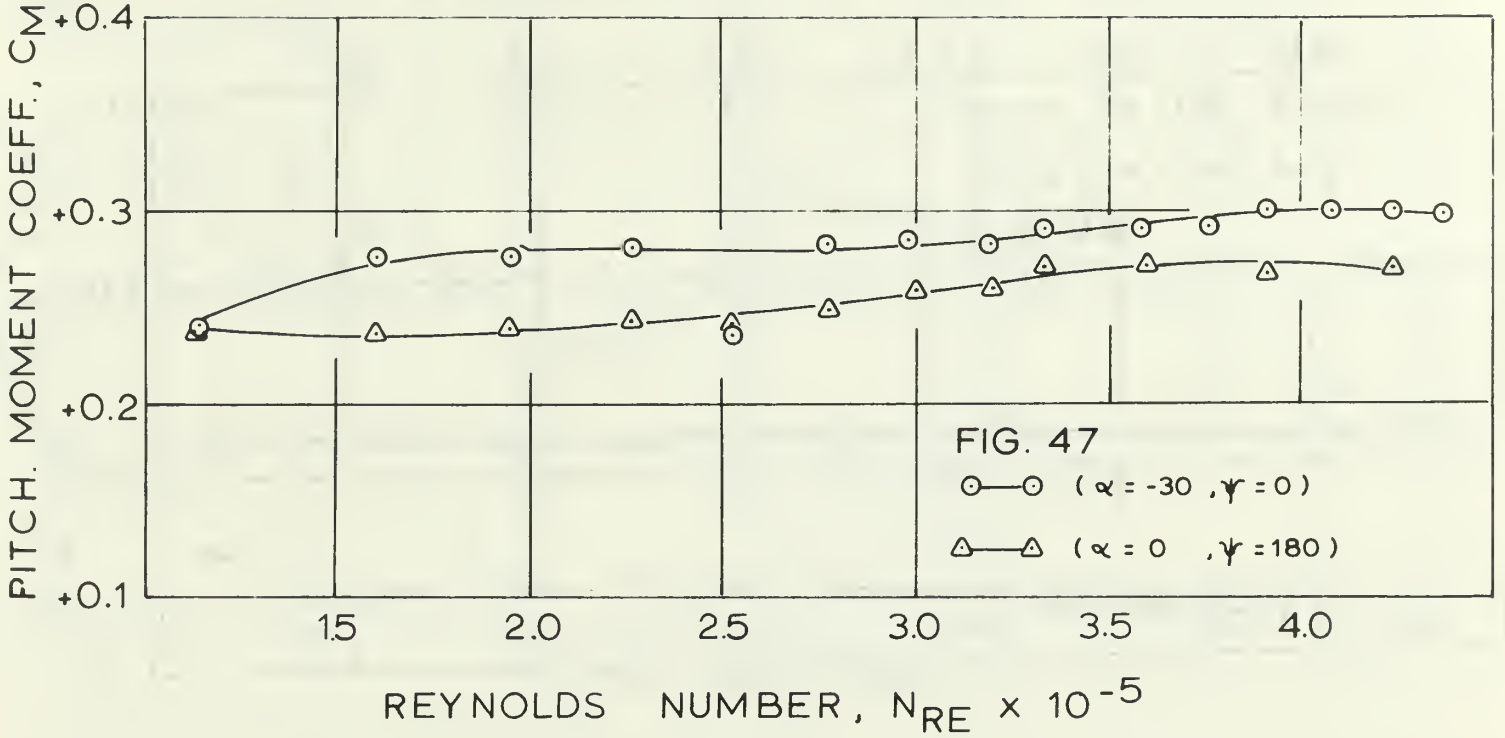
PITCH. MOMENT COEFF., C_M
+0.4
+0.3
+0.2
+0.1
1.5
2.0
2.5
3.0
3.5
4.0
REYNOLDS NUMBER, $N_{RE} \times 10^{-5}$
FIG. 47
(α = -30 , ψ = 0)
(α = 0 , ψ = 180)

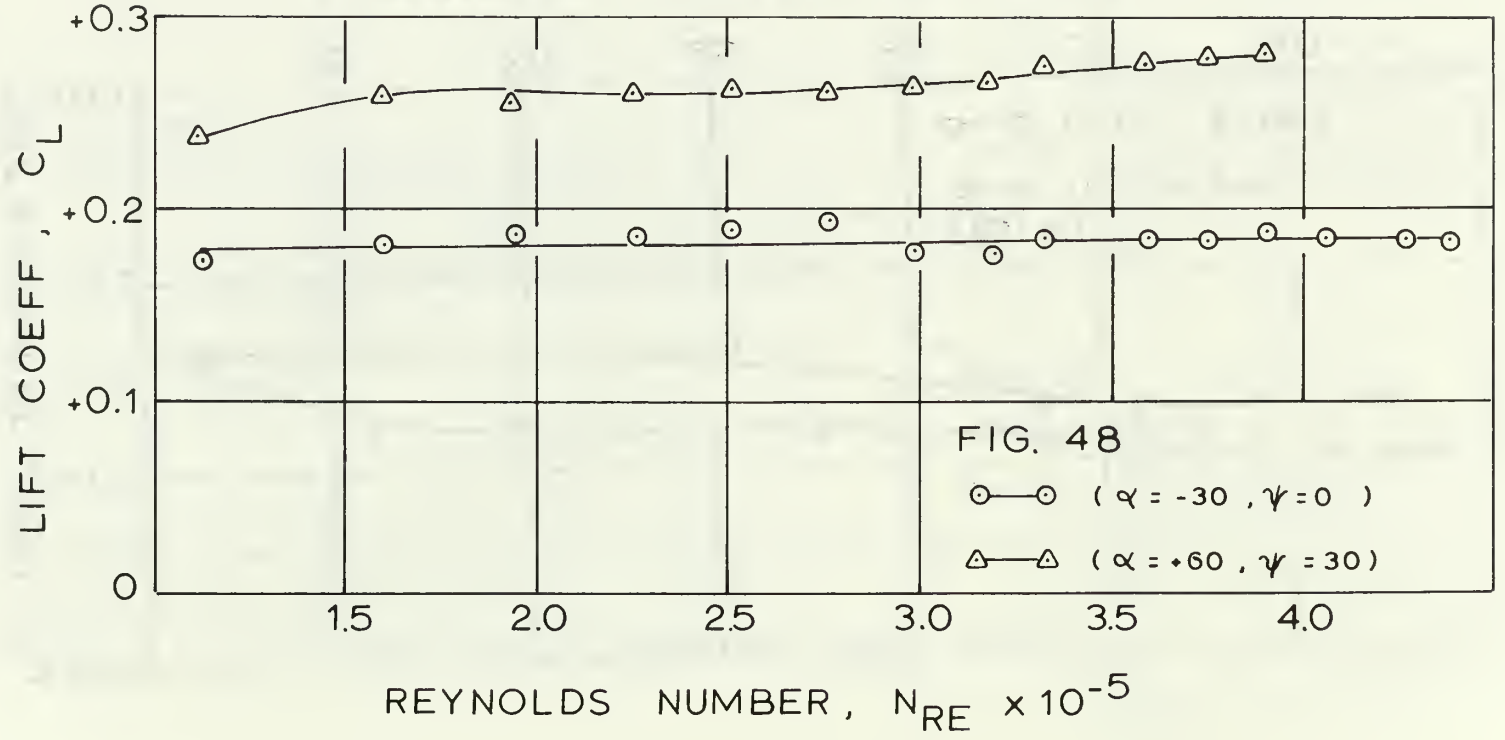
+0.3
+0.2
+0.1
0
LIFT COEFF , C_L
1.5
2.0
2.5
3.0
3.5
4.0
REYNOLDS NUMBER , $N_{RE} \times 10^{-5}$
FIG. 48
(α = -30 , ψ = 0)
(α = +60 , ψ = 30)

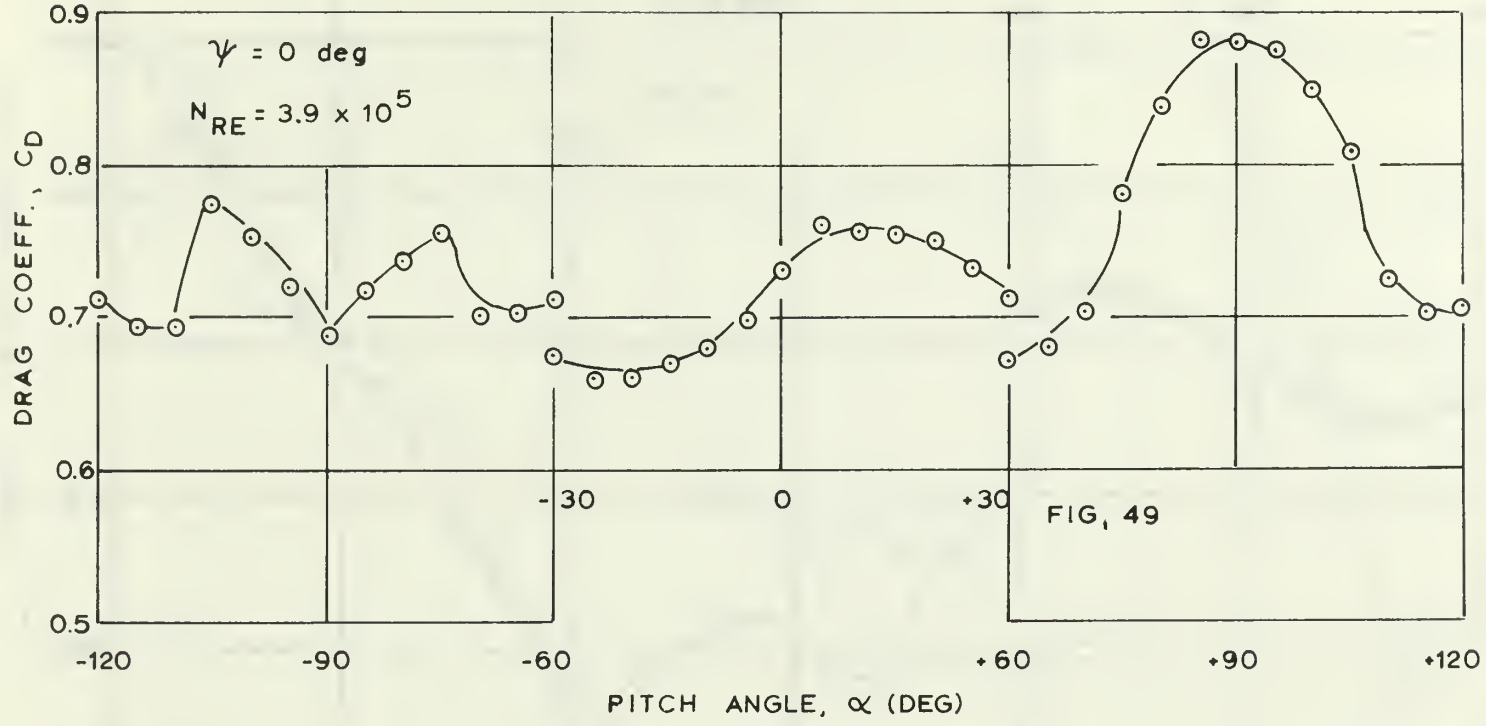
ψ = 0 deg
N_{RE} = 3.9 x 10^5
DRAG COEFF., C_D
0.9
0.8
0.7
0.6
0.5
-120
-90
-60
-30
0
+30
+60
+90
+120
PITCH ANGLE, α (DEG)

FIG. 49

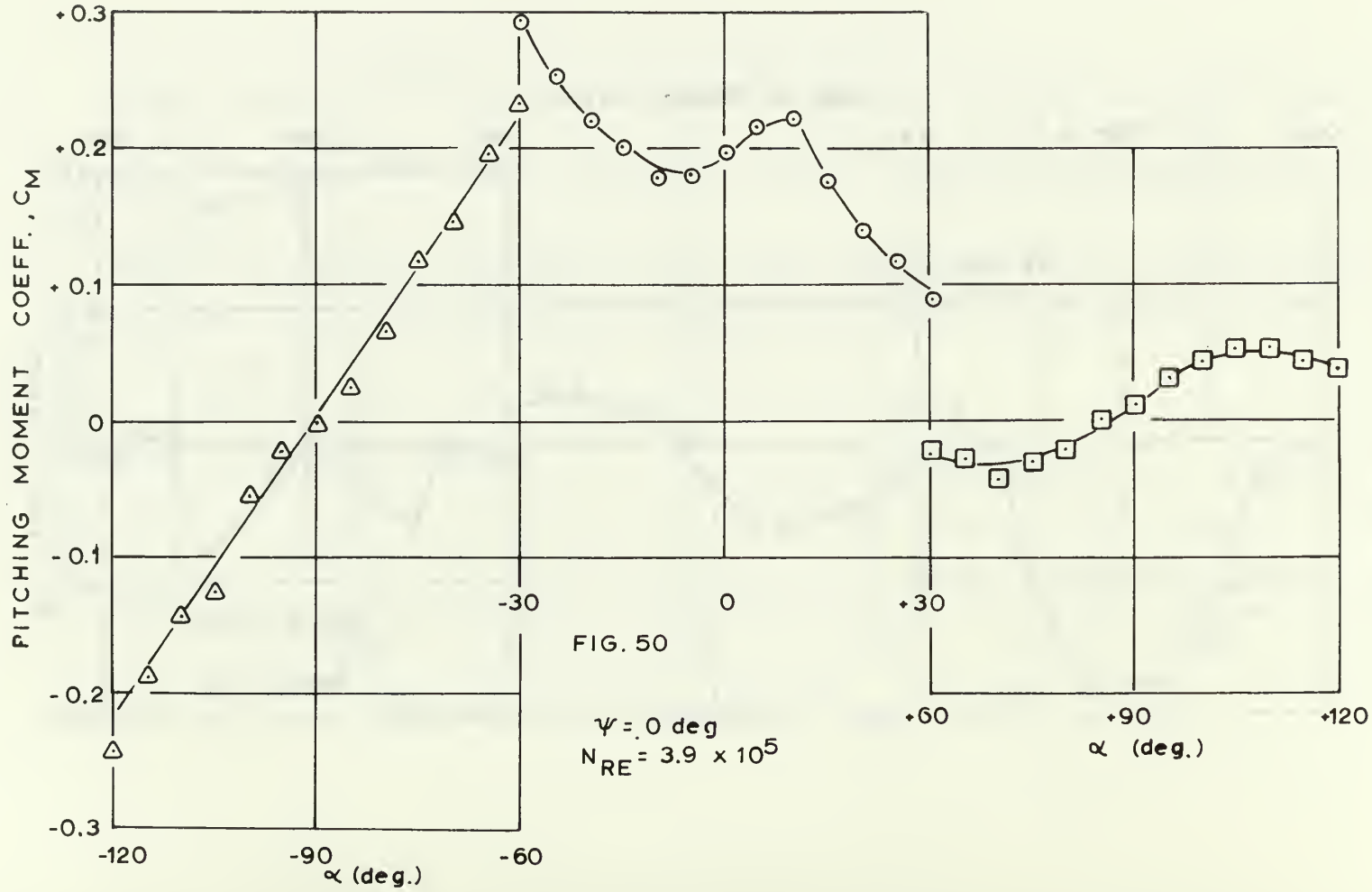
+0.3
+0.2
+0.1
0
-0.1
-0.2
-0.3
PITCHING MOMENT COEFF., C_M
-120
-90
-60
-30
0
+30
+60
+90
+120
α (deg.)
α (deg.)
ψ = 0 deg
N_{RE} = 3.9 x 10^5

FIG. 50

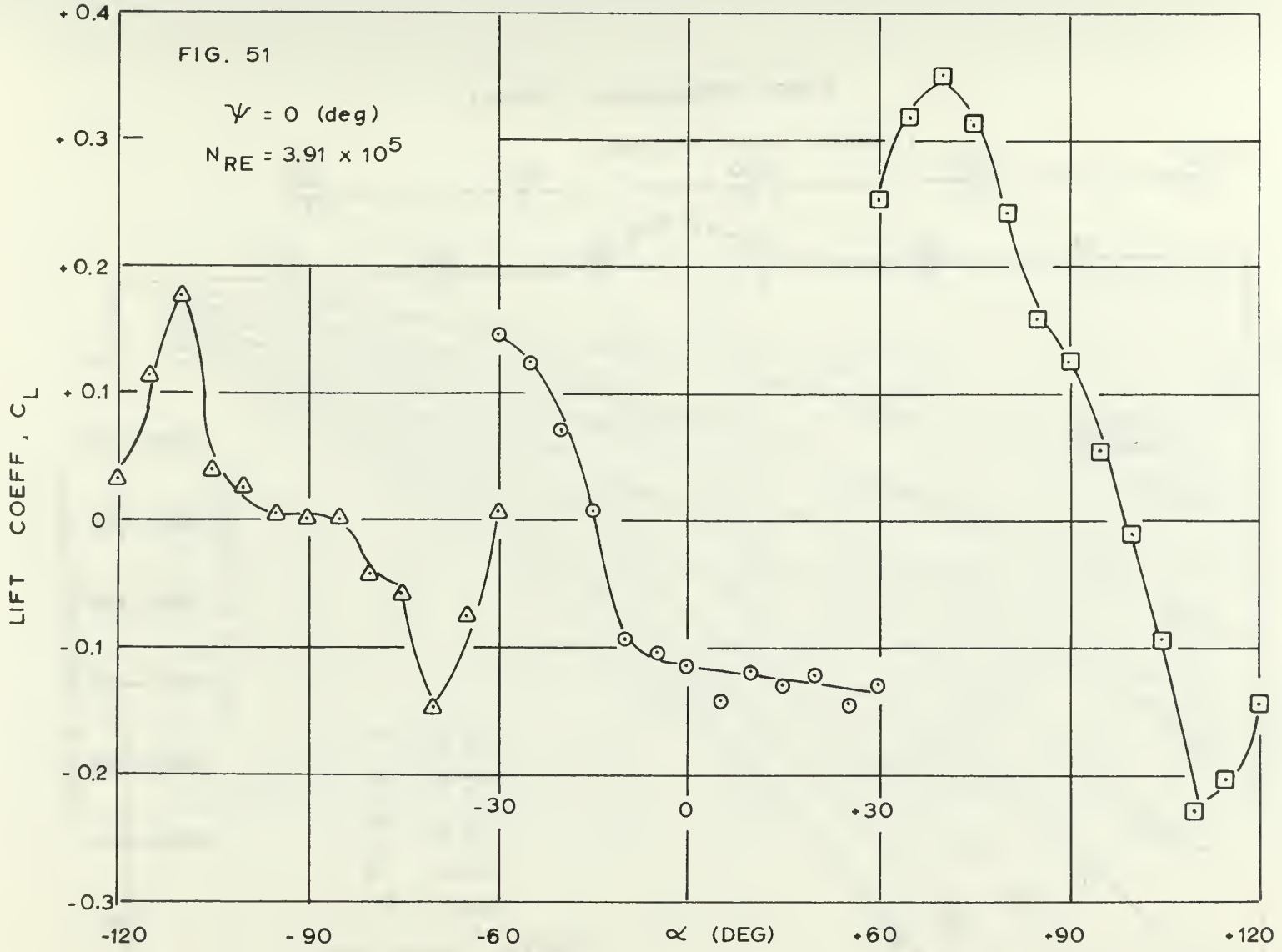
FIG. 51
Ψ = 0 (deg)
N_RE = 3.91 x 10^5
+0.4
+0.3
+0.2
+0.1
0
-0.1
-0.2
-0.3
LIFT COEFF., C_L
-120
-90
-60
-30
0
+30
+60
+90
+120
∝ (DEG)

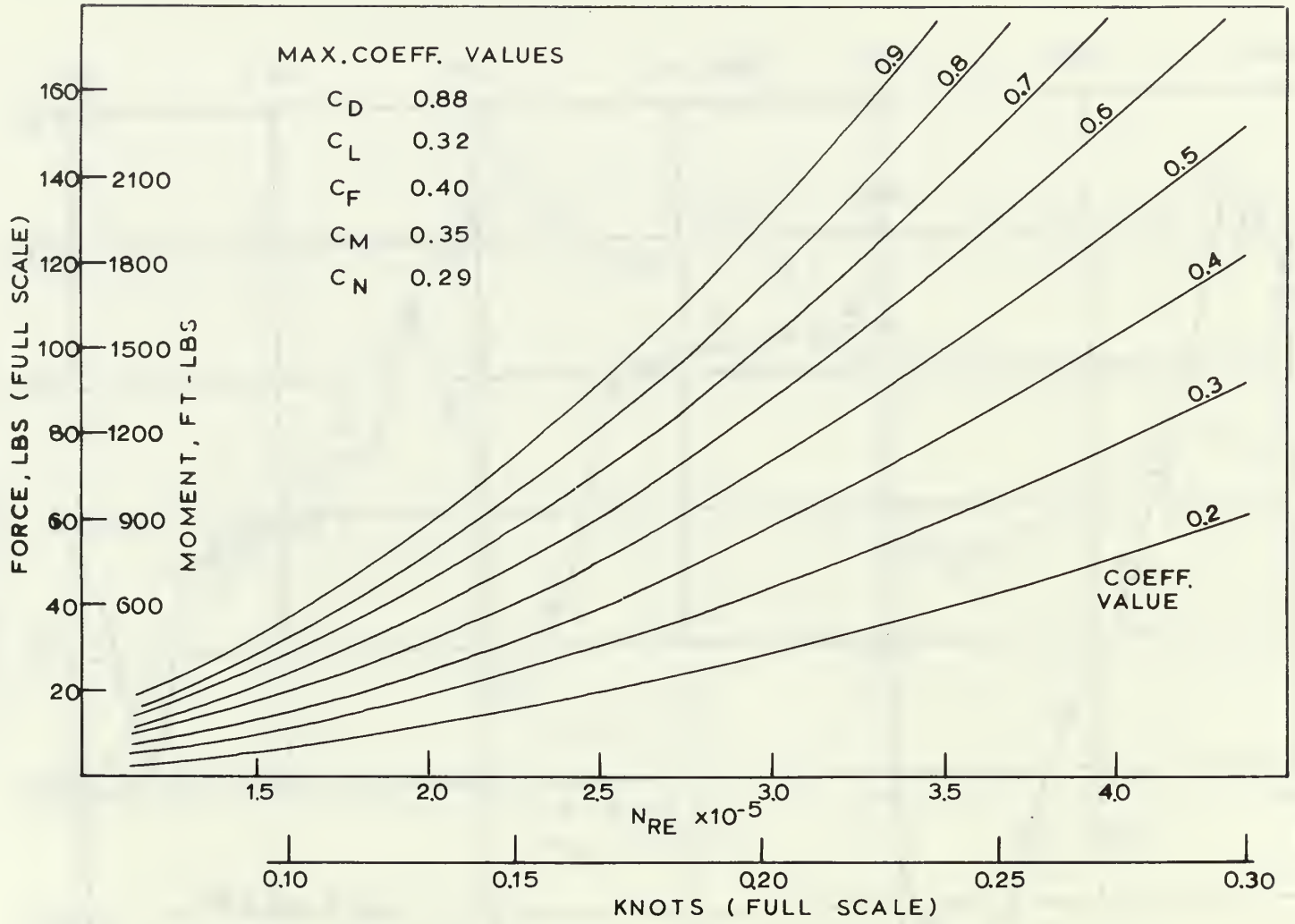

FIG. 52 CONVERSION SCALE

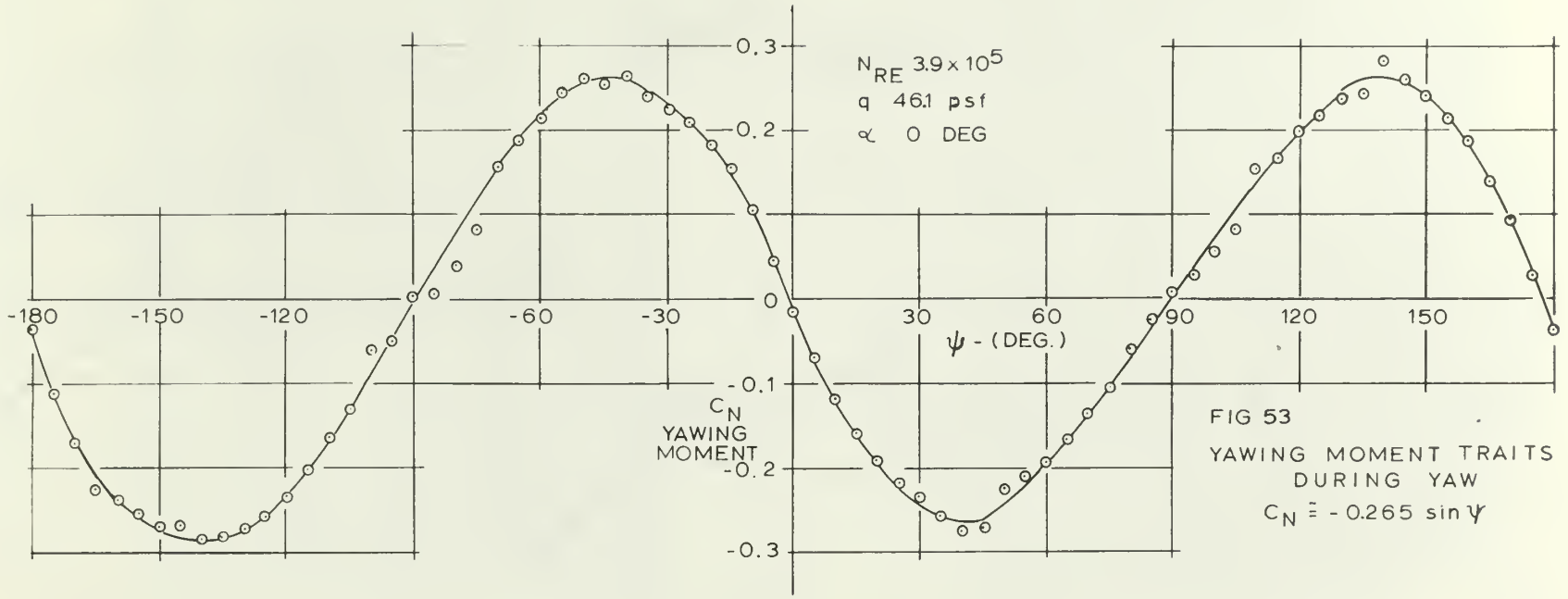

FIG 53

YAWING MOMENT TRAITS
DURING YAW

$C_N \doteq -0.265 \sin\psi$

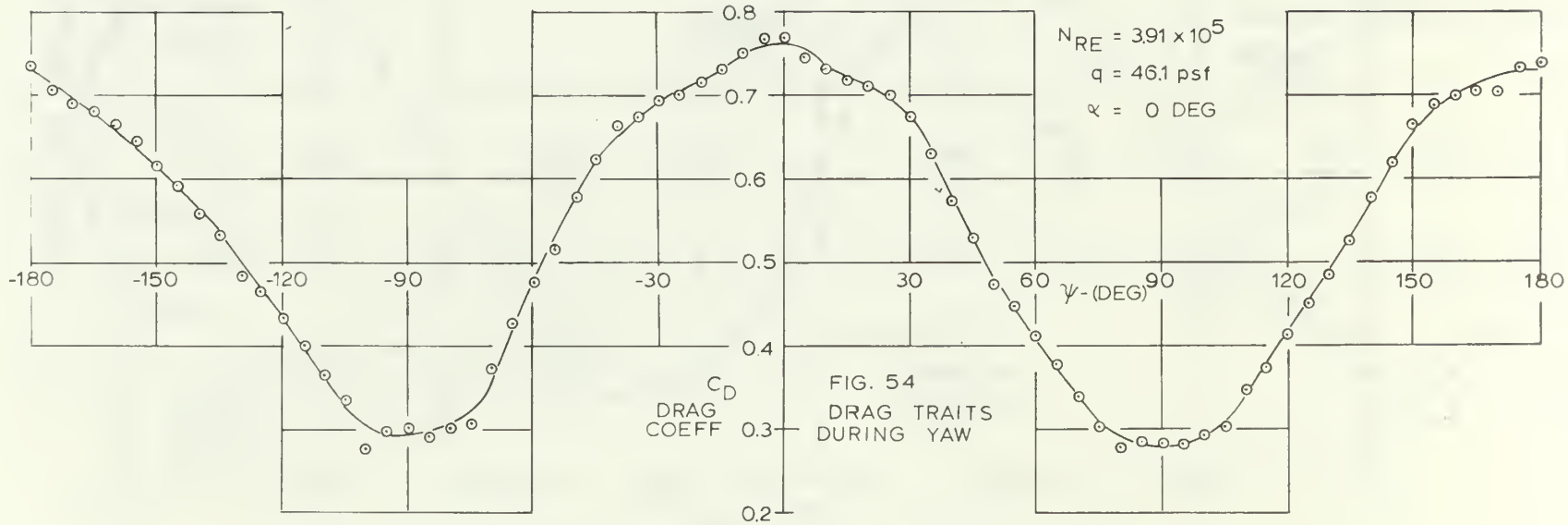

FIG. 54
DRAG TRAITS
DURING YAW

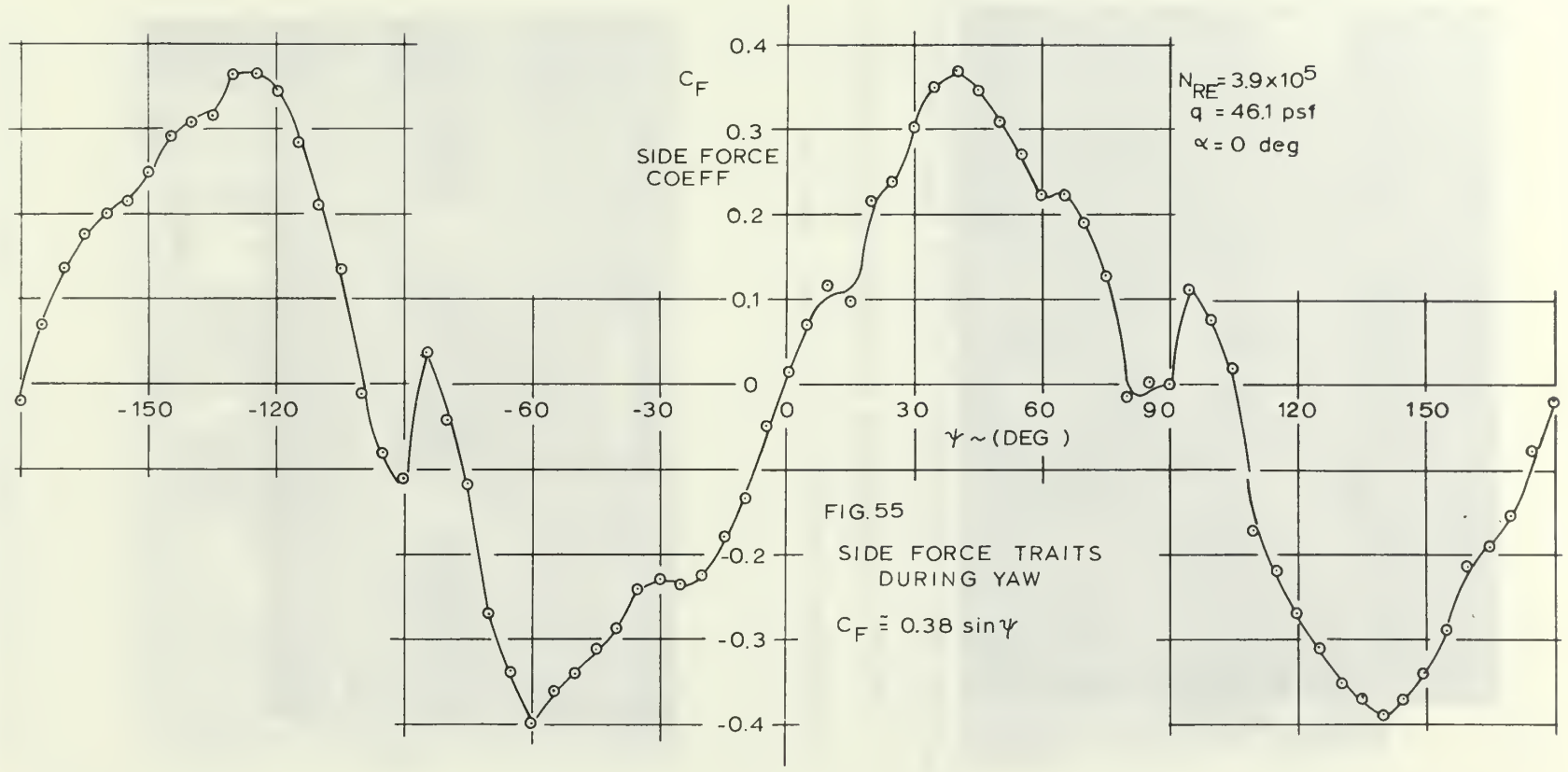

FIG. 55

SIDE FORCE TRAITS
DURING YAW

$C_F \cong 0.38 \sin\psi$

Fig. 56 - Photograph of the West Coast Research 48 in. x 60 in. wind tunnel, showing support beams for wire attachment exterior to the test section

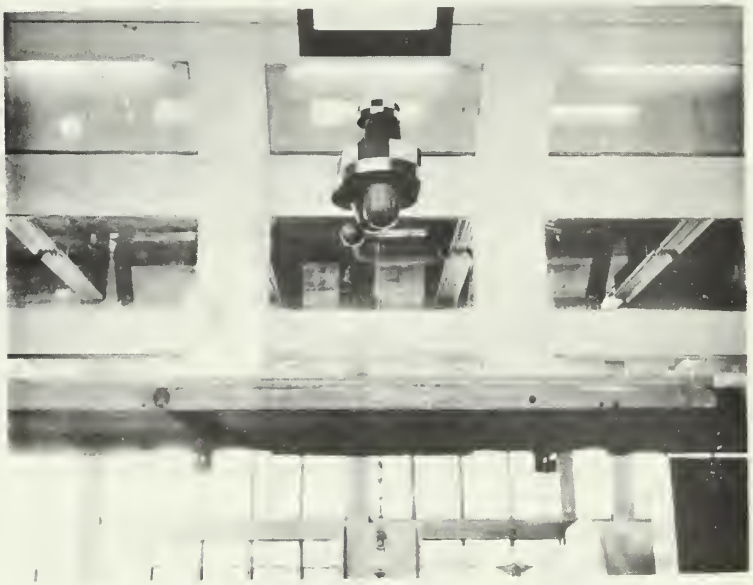

Fig. 57 - The dynamic model in the test section, side view

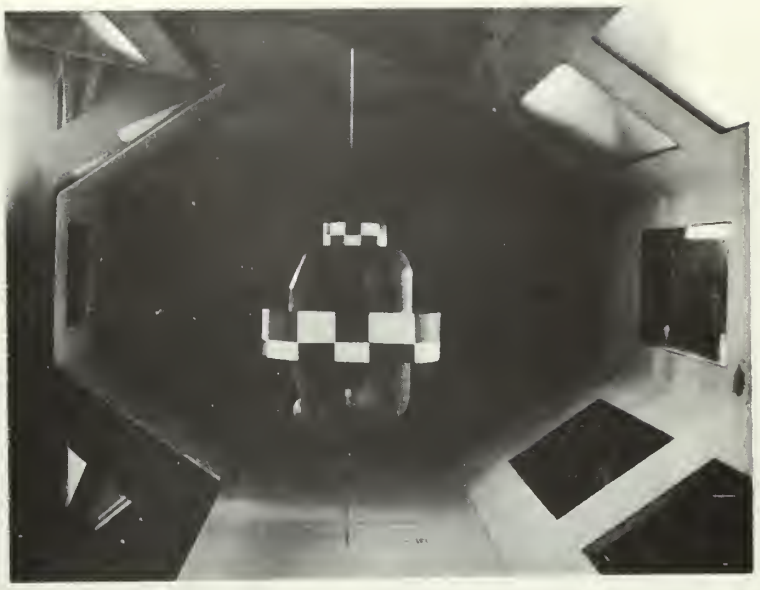

Fig. 58 - Photograph of the dynamic model in the test section, view from downstream

Fig. 59 - Close-up of the dynamic model

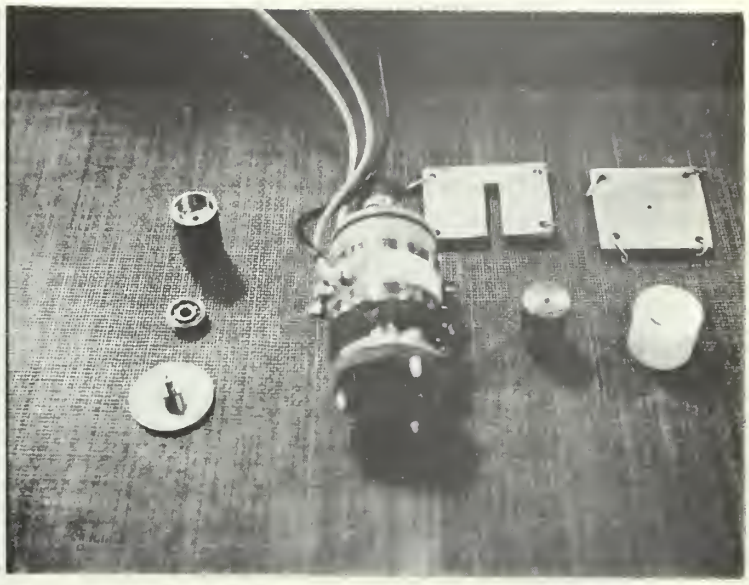

Fig. 60 - Photograph of dynamic model instrumentation hardware and bearings

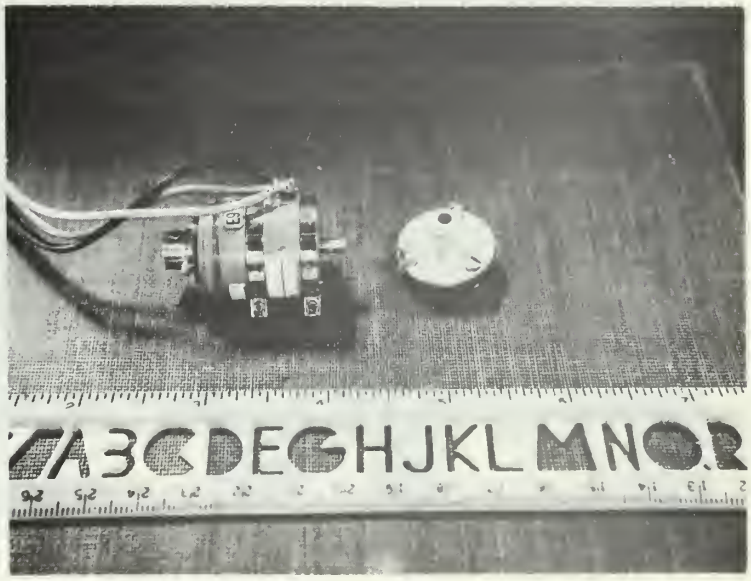

Fig. 61 - Photograph of the modified potentiometer used in dynamic model instrumentation

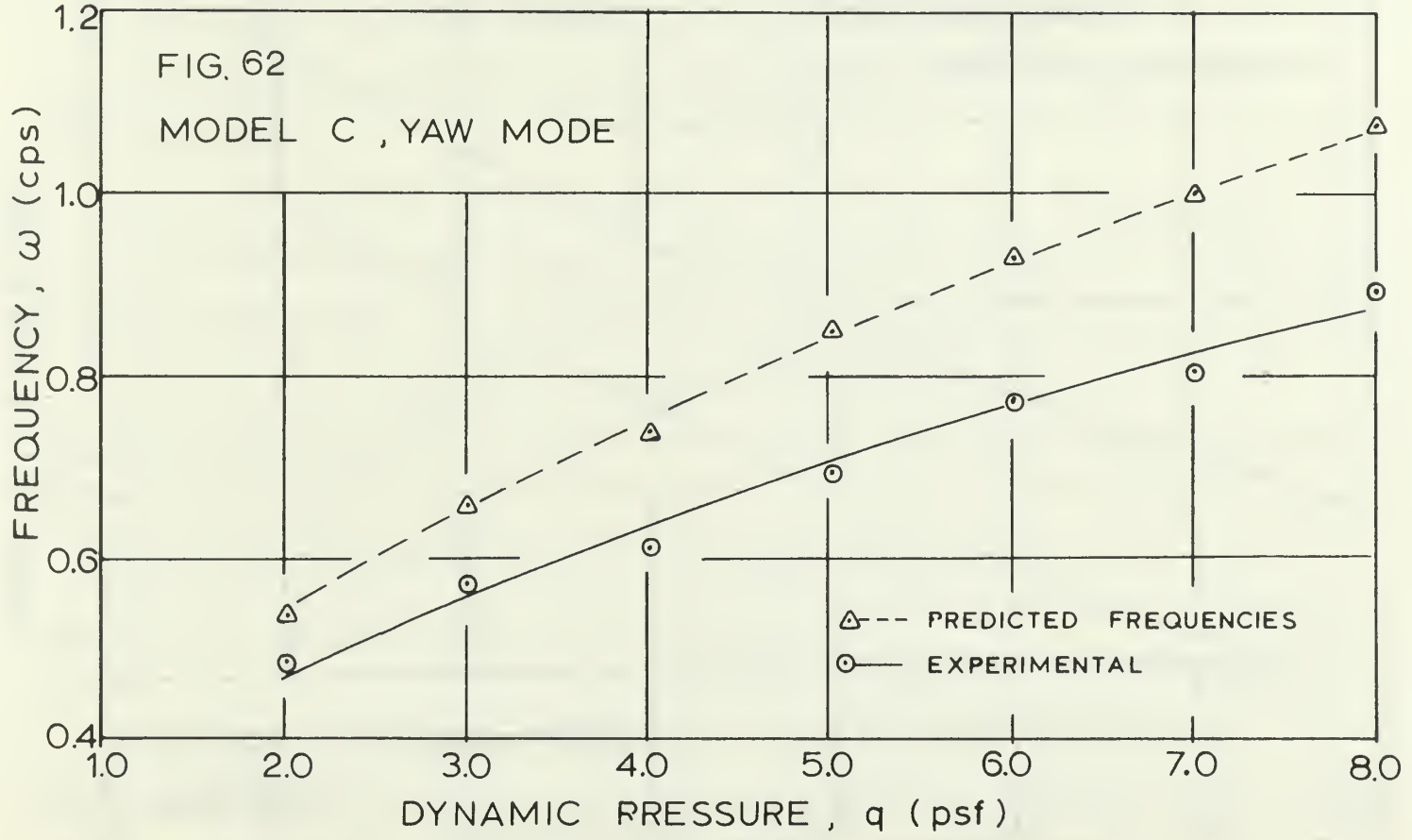
FIG. 62
MODEL C , YAW MODE
FREQUENCY, ω (cps)
1.2
1.0
0.8
0.6
0.4
1.0
2.0
3.0
4.0
5.0
6.0
7.0
8.0
DYNAMIC PRESSURE , q (psf)
PREDICTED FREQUENCIES
EXPERIMENTAL

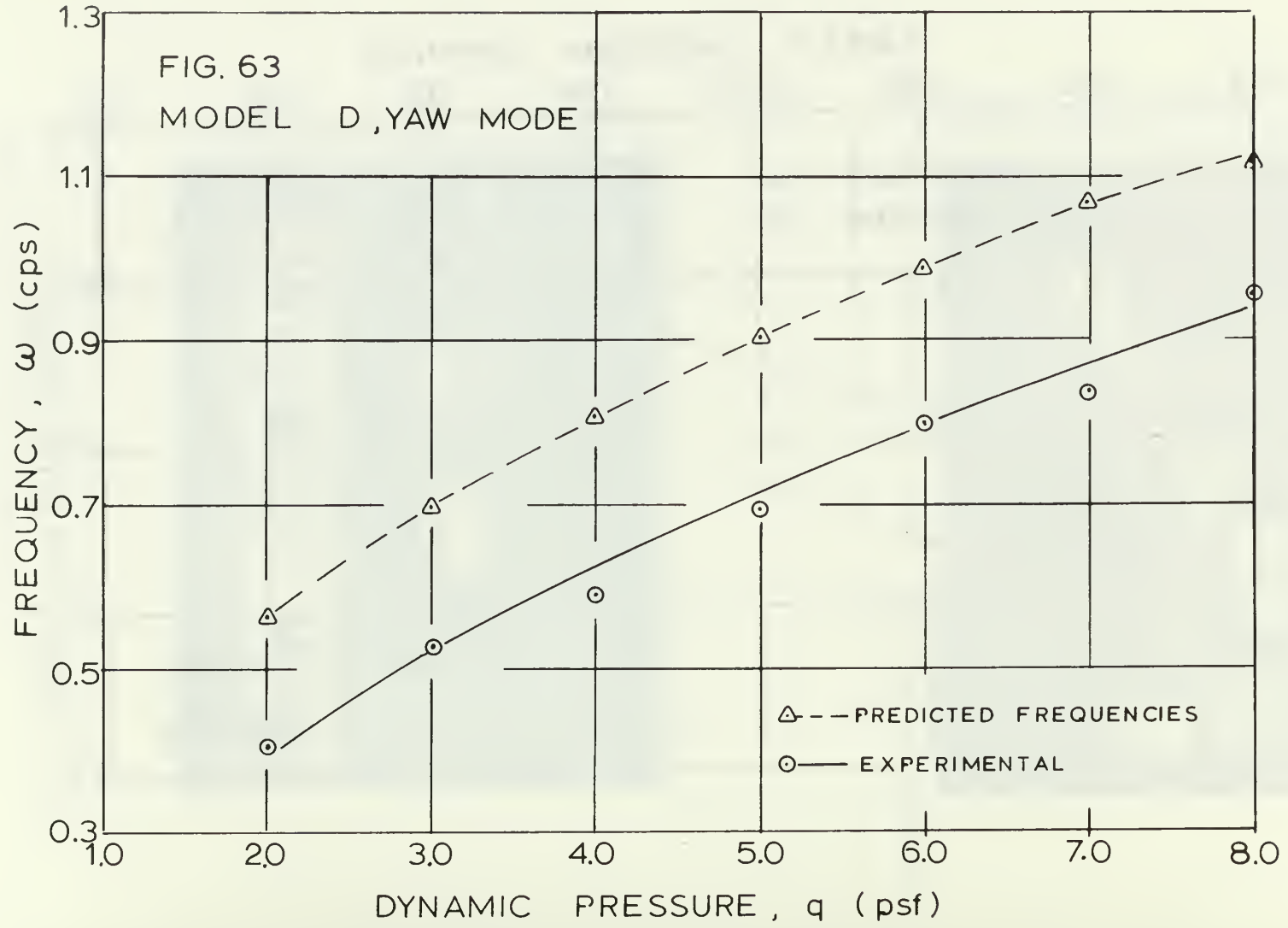
FIG. 63
MODEL D, YAW MODE
FREQUENCY, ω (cps)
1.3
1.1
0.9
0.7
0.5
0.3
1.0
2.0
3.0
4.0
5.0
6.0
7.0
8.0
DYNAMIC PRESSURE, q (psf)
PREDICTED FREQUENCIES
EXPERIMENTAL

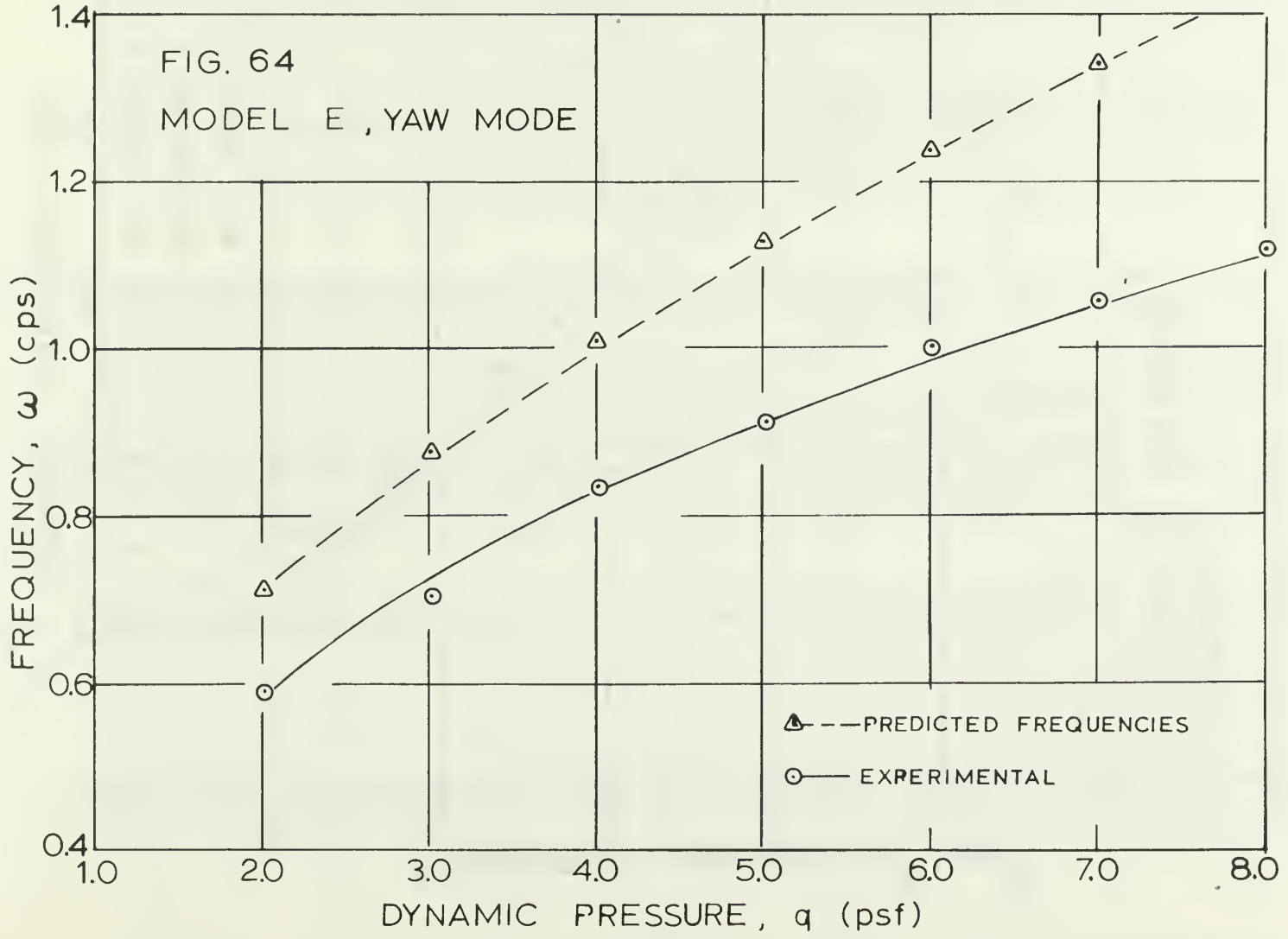
FIG. 64
MODEL E , YAW MODE
FREQUENCY, ω (cps)
1.4
1.2
1.0
0.8
0.6
0.4
1.0
2.0
3.0
4.0
5.0
6.0
7.0
8.0
DYNAMIC PRESSURE, q (psf)
PREDICTED FREQUENCIES
EXPERIMENTAL

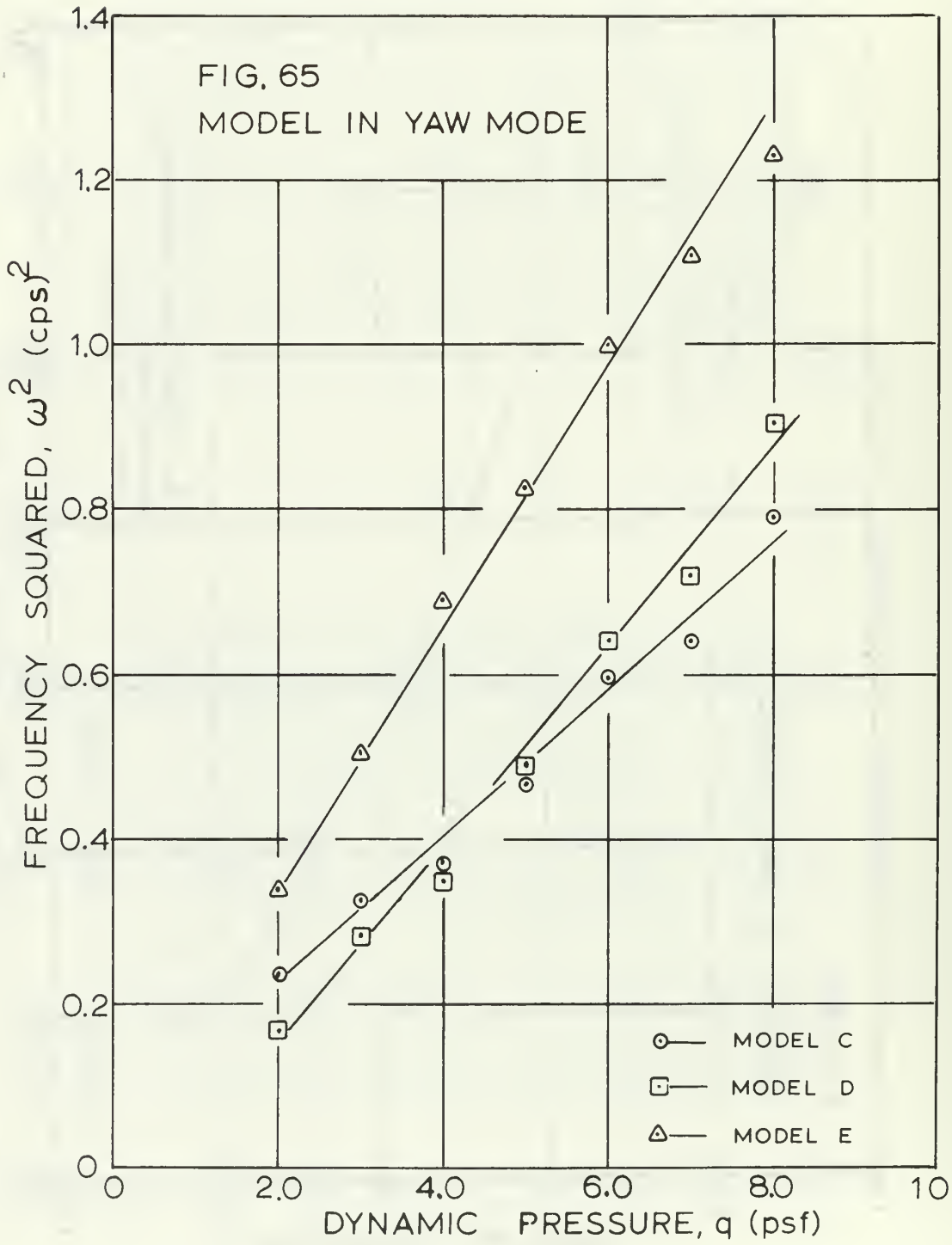
FIG. 65
MODEL IN YAW MODE
FREQUENCY SQUARED, ω^2 (cps)^2
1.4
1.2
1.0
0.8
0.6
0.4
0.2
0
0
2.0
4.0
6.0
8.0
10
DYNAMIC PRESSURE, q (psf)
MODEL C
MODEL D
MODEL E

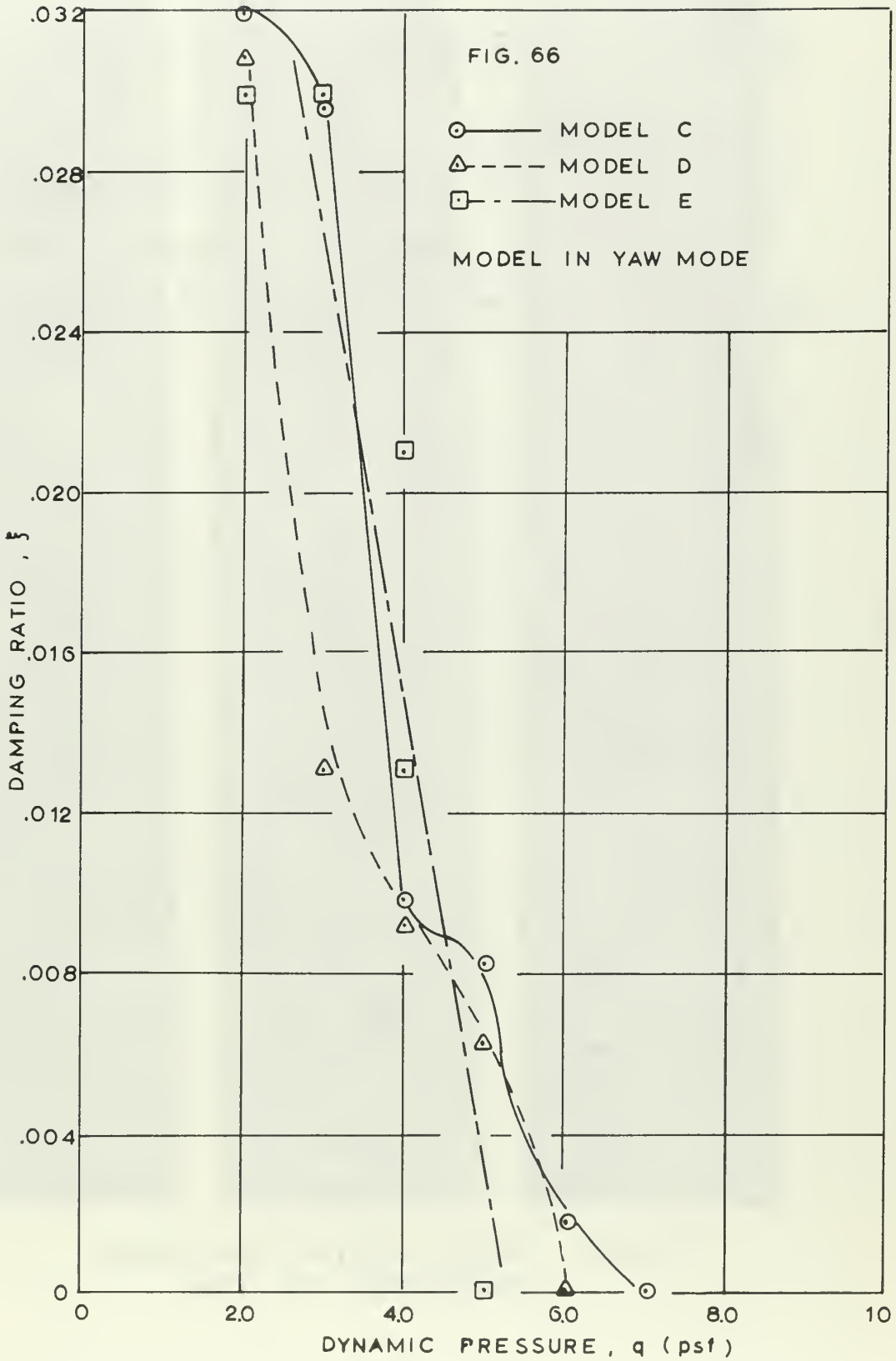
FIG. 66
MODEL C
MODEL D
MODEL E
MODEL IN YAW MODE
.032
.028
.024
.020
.016
.012
.008
.004
0
DAMPING RATIO , ξ
0
2.0
4.0
6.0
8.0
10
DYNAMIC PRESSURE , q (psf)

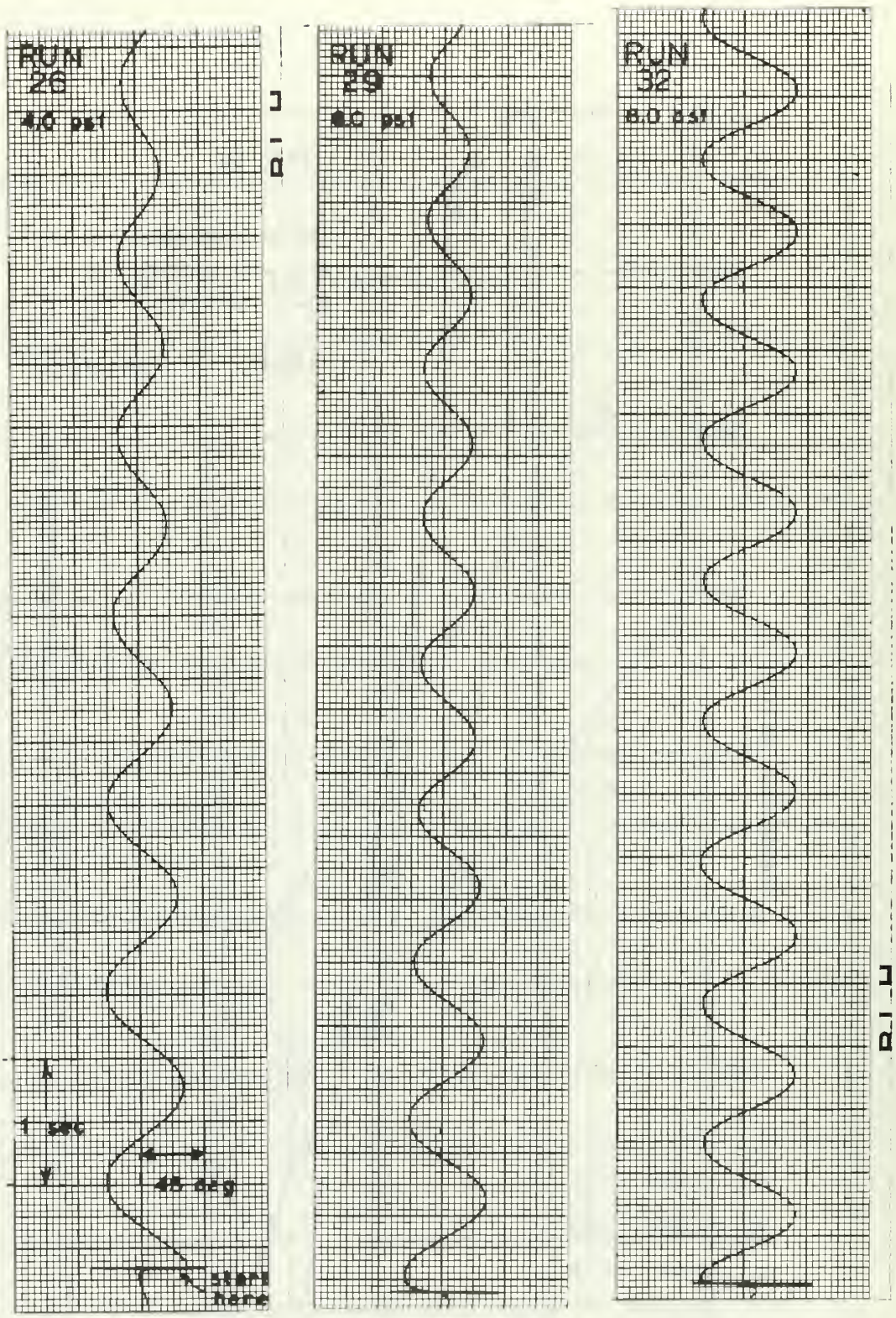

FIG. 67 TIME HISTORY OF FREE VIBRATION IN YAW

BIBLIOGRAPHY

1. Naval Civil Engineering Laboratory Report CR 68.012, Concept Development of Manned Underwater Station, by David W. Carreau, 1 July 1968

2. Parkinson, G.V., and Smith, J.D., The Square Prism as an Aeroelastic Non-Linear Oscillator, Quart. J. Mech. and Appl. Math., Vol. 17, Part 2, pp. 225-239, 1964

3. Pope, A., Wind-Tunnel Testing, Wiley, 1947

4. Bisplinghoff, R.L., Ashley, H., Halfman, R.L., Aeroelasticity, Addison - Wesley, 1955

INITIAL DISTRIBUTION LIST

		No. Copies
1.	Defense Documentation Center Cameron Station Alexandria, Virginia 22314	20
2.	Library, Code 0212 Naval Postgraduate School Monterey, California 93940	2
3.	Commander, Naval Air Systems Command Department of the Navy Washington, D. C. 20360	1
4.	Chairman Department of Aeronautics Naval Postgraduate School Monterey, California 93940	1
5.	Professor Louis V. Schmidt Department of Aeronautics Naval Postgraduate School Monterey, California 93940	17
6.	Lt. Robert L. Ditchey, USN 617 East Broad Street Tamaqua, Pennsylvania 18252	1

Security Classification

DOCUMENT CONTROL DATA - R & D

(Security classification of title, body of abstract and indexing annotation must be entered when the overall report is classified)

1. ORIGINATING ACTIVITY *(Corporate author)*
Naval Postgraduate School
Monterey, California 93940

2a. REPORT SECURITY CLASSIFICATION
Unclassified

2b. GROUP

3. REPORT TITLE
A Wind Tunnel Investigation of the Hydrodynamic Stability of a Manned Underwater Station in Ocean Currents

4. DESCRIPTIVE NOTES *(Type of report and inclusive dates)*
Master's Thesis; (October 1969)

5. AUTHOR(S) *(First name, middle initial, last name)*
Robert L. Ditchey

6. REPORT DATE	7a. TOTAL NO. OF PAGES	7b. NO. OF REFS
October 1969	98	4

8a. CONTRACT OR GRANT NO.

b. PROJECT NO.

c.

d.

9a. ORIGINATOR'S REPORT NUMBER(S)

9b. OTHER REPORT NO(S) *(Any other numbers that may be assigned this report)*

10. DISTRIBUTION STATEMENT
This document has been approved for public release and sale; its distribution is unlimited.

11. SUPPLEMENTARY NOTES

12. SPONSORING MILITARY ACTIVITY
Naval Postgraduate School
Monterey, California 93940

13. ABSTRACT

The hydrodynamic stability of an underwater station was studied using wind tunnel models. Rigid model force and moment coefficients were obtained for various orientations of the station in three dimensions. The unsteady motion of the station in cross currents was investigated with a dynamically similar model. Color 8 mm pictures and amplitude-time traces of the unsteady motion were obtained.

DD FORM 1 NOV 68 1473 (PAGE 1)
S/N 0101-807-6811

Security Classification

A-31406

14 KEY WORDS	LINK A		LINK B		LINK C	
	ROLE	WT	ROLE	WT	ROLE	WT
Hydrodynamic Stability						
Manned Underwater Station						
Dynamically Similar Model						

Thesis
D585
c.1

113186

Ditchey

A win tunnel investigation of the hydrodynamic stability of a manned under water station in ocean currents.